

## Response to reviewers

We thank the reviewers for their comments. Detailed responses are given below.

### Response to reviewer #1

#### Major points:

1. May I suggest to highlight 'numerical simulation' in the title?

*This is a good idea. The title has been changed to "Two-dimensional numerical simulations of shoaling internal solitary waves at the ASIAEX site in the South China Sea".*

2. The abstract: it is mostly about 'what has been done' in the work, not 'what has been found'. It would be nice if the authors could consider improving this.

*The abstract has been rewritten:*

*"The interaction of barotropic tides with Luzon Strait topography generates some of the world's largest internal solitary waves which eventually shoal and dissipate on the western side of the north South China Sea. Two-dimensional numerical simulations of the shoaling of a single internal solitary wave at the site of the Asian Seas International Acoustic Experiment have been undertaken in order to investigate the sensitivity of the shoaling process to the stratification and the underlying bathymetry, and to explore the influence of rotation. The bulk of the simulations are inviscid however exploratory simulations using a vertical eddy-viscosity confined to a near bottom layer, along with a no-slip boundary condition, suggest that viscous effects may become important in water shallower than about 200 m. A shoaling solitary wave fissions into several waves. At depths of 200-300 m the front of the leading waves become nearly parallel to the bottom and develop a very steep back as has been observed. The leading waves are followed by waves of elevation (pedestals) that are conjugate to the waves of depression ahead and behind them. Horizontal resolutions of at least 50 m are required to simulate these well. Wave breaking was found to occur behind the second or third of the leading solitary waves, never at the back of the leading wave. Comparisons of the shoaling of waves started at depths of 1000 and 3000 m show significant differences and the shoaling waves can be significantly non-adiabatic even at depths greater than 2000 m. When waves reach a depth of 200 m their amplitudes can be more than 50% larger than the largest possible solitary wave at that depth. The shoaling behaviour is sensitive to the presence of small scale features in the bathymetry: a 200 m high bump at 700 m depth can result in the generation of many mode-two waves and of higher mode waves.*

*Sensitivity to the stratification is considered by using three stratifications based on summer observations. They primarily differ in the depth of the thermocline. The generation of mode-two waves and the behaviour of the waves in shallow water is sensitive to this depth. Rotation affects the shoaling waves by reducing the amplitude of the leading waves via the radiation of long trailing inertia-gravity waves. The nonlinear-dispersive evolution of these inertia-gravity waves results in the formation of secondary mode-one wave packets. ”*

3. P1166, L8-16: Please improve this paragraph; the first citation and the third citation have a similar story.

*Done. The paragraph now starts with:*

*“Liu et al (1998) demonstrated, with a two-layer Gardner equation model that includes cubic nonlinearity, that ISW depressions are transformed into a train of ISWs of elevation as they propagate over sloping topography into shallower water where the upper layer is thinner than the lower layer, as did Orr and Mignerey (2003) who based their simulations on observations from the ASIAEX site. Recently Grimshaw et al (2014) used the Ostrovsky equation to investigate the effects of rotation on the evolution of shoaling solitary waves. They too included a cubic nonlinear term. Their simulations were based on bathymetry and continuous stratifications observed in the South China Sea. They found that a significant consequence of rotation was the formation of a secondary trailing wave packet associated with nonlinear steepening of the radiated inertia gravity waves. ...”*

4. About rotation: are the authors aware of the recent work by Grimshaw et al. (2014)? They studied the combined effect of rotation and shoaling topography on the propagation of internal solitary waves in the South China Sea. A major finding is that the combined effect results in the formation of a secondary wave train after the leading wave passes by the shelf break. This secondary wave train, although being less pronounced, also appears in Fig. 18. The authors may want to discuss a bit around this. Grimshaw et al. (2014) also did some sensitivity runs which are also relevant to the topic of this paper.

*The authors were not aware of this paper at the time of submission. This reference has been added along with appropriate discussion. In the initial version of the paper figure 21c showed a mode-one solitary wave packet that was formed through rotational effects. We have replaced former figures 20 and 21 with new figures (figures 17 and 18) which clearly show the formation of secondary wave packets as reported by Grimshaw et al. We have also modified figure 15 (figure 18 in original manuscript) by adding a new panel comparing isopycnal heights at a later time for one case which clearly shows the secondary wave packet.*

*Part of the additions include the following sentences in section 3.6:*

*“The wave of elevation between  $x = 30$  and  $50$  km is larger in the rotating case (surface currents are twice as strong) and in the rotating case it subsequently steepens and forms a secondary packet of short waves (between  $x = 67$  to  $70$  km at  $t = 45$  h, Fig. 15c) which is not present in the non-rotating case. Such wave packets were reported by Grimshaw et al, (2014).”*

**Minor points:**

- P1164, L3: solitary wave train.  
*Fixed.*
- P1164, L15: in situ observations?  
*Fixed.*
- P1167, L25: grammatical error.  
*Fixed.*
- P1169, L9–12: this should appear in the caption.  
*Sentences removed. Explanation in caption.*
- P1170, L27: is approached they  
*Fixed.*
- P1171, L18: 45.4 m  
*Fixed.*
- P1171, L18: what are Case 2 and 3? Table 3 is not introduced before this.  
*Fixed. An introductory paragraph describing the table has been added. Tables 2 and 3 have been re-ordered.*
- P1174, L21: too wide  
*Fixed.*
- P1174, L26: please explain a bit about  $J=200$ .  
 *$J$  is the number of grid cells in the vertical. Mention of this is now made in section 2.1 where the model is introduced along with a comment about vertically varying resolution.*
- P1180, L5: grammatical error.  
*Revised.*
- P1181, L12: steeper than  
*Fixed.*
- P1182, L23: the wave has reached  
*Fixed.*

- P1184, L8: e.g.  $t_x=18$ ?  
*Fixed.*
- P1186, L16: consider case with an specify which case?  
*Text has been modified.*
- P1186, L27: Incomplete sentence; informal in a paper.  
*Sentence modified.*
- P1187, L12: do the modeled characteristics of the second mode match those of observations (e.g., amplitude, location, etc.)? One may not expect a good agreement with such an idealized simulation, but it would be helpful to discuss it a bit.

*Only one mode-two wave was reported in the ASIAEX field program (see Lynch et al (2004)). Most of the observations of mode-two waves were obtained in the VANS/WISE field program which was conducted in 2005 and 2006 at a nearby location. These observations were from a mooring along the 350 m isobath and we do see them at this depth in the simulations. We have extended the discussion of the mode-two observations in section 4. It now reads*

*“During the ASIAEX program only one mode-two wave was observed (Lynch et al, 2004). In a pilot program (Yang et al, 2004) observed a single mode-two wave in water 426 m deep. Yang et al (2009, 2010) analyzed mooring data obtained during the VANS/WISE program which was conducted in 2005 and 2006 in the vicinity of the ASIAEX field program. Data from a mooring deployed along the 350 m isobath was analyzed showed the occurrence of many mode-two waves. They appeared in two forms: convex mode-two waves in which there is a bulge in the thermocline with isotherms raised/lowered in the upper/lower part of the water column, and concave mode-two waves with isotherms displaced in the opposite directions. Convex mode-two waves were by far the most common. The mode-two waves trailed mode-one waves suggesting that they were generated via the adjustment of shoaling mode-one waves (Yang et al (2009). Stratification and seasonal variations played a role in generation of mode-two ISWs with mode-two waves more common in winter (Yang et al, 2009). Our simulations also showed the formation of both convex and concave mode-two waves which evolved from the shoaling mode-one wave, as observed by Yang et al (2009, 2010). In the simulations they were present at the depths of the observed waves. Their presence and amplitude were sensitive to the stratification and to rotational effects. The shallow bump on bathymetry  $h_{15}$  led to the generation of a mode-two wave train and made the mode-two ISWs more prominent (see Fig. 13). The generation mechanisms of mode-two ISWs, their frequency of occurrence, and locations on the continental shelf require further study.”*



- P1189, L9: I think it is northeastern South China Sea.  
*Yes. We were thinking of the western side of that region of the South China Sea. Text has been modified.*
- P1190, L28: as they shoal into  
*Fixed.*
- P1191, L25: 120 m  
*Fixed.*

### **Tables/figures:**

- Table 1: please explain the variables in the first row.  
*Done.*
- Table 2: the last sentence is incomplete.  
*Sentence has been revised.*
- Table 3: I do not see any  $\nu$  in the table and delete one for in the middle of the caption.  
*The  $\nu$  was meant to indicate cases for which sets of three runs were done with viscosity. Actual case numbers have an additional  $n$  to indicate the value of the viscosity. The caption has been modified to clarify this.*
- Fig. 1: please add information of isobaths and color bar.  
*Done.*
- Fig. 2: the grey lines in panels b and c are nearly invisible.  
*They have been darkened and thickened.*
- Fig. 3: please specify in the caption that panels a and b have different y-axis scales. I also found panel c not very readable and not necessary. Can the authors consider removing it?  
*We have removed panel (b) and kept panel (c). Plotting three panels in a single row stretches the plots vertically so they are more readable.*
- Fig. 5: please specify in the caption that the scale of y-axis in panels a and b is different.  
*Done.*
- Fig. 9: please indicate in the figure the location of the mode-two wave.  
*Done.*

- Fig. 10: 1) Line 4 in the caption: 100 m (dotted); 2) incomplete sentences in the caption; 3) the last sentence in the caption: if the curve of the higher vertical resolution results is indistinguishable from the solid curve, I don't think it necessary to actually overlie and describe this curve; 4) please add legend in the panels. I have to refer back to the caption very frequently during reading; 5) It seems that the information in the caption is inconsistent with that described in the text.

*This figure has been replaced and the caption rewritten. A new panel has been added including results from a simulation using 16 m resolution. Unfortunately we have not been able to redo all of the simulations at the higher resolution.*

- Fig. 12a: Is the magnitude of the y-axis correct?  
*It should have been GJ/m, not MJ/m. Has been corrected.*
- Fig. 13: please try to enhance the readability this figure.  
*We have changed the blue and green colours to improve readability and have added a legend.*

## Response to reviewer #2

1. My primary criticism is they didn't really do enough when it comes to comparing the results to observations. The authors went to great lengths to accurately reproduce the bottom slope, topographic bumps, etc. of the SCS ASIAEX region, but then they never really got round to going back and comparing the model output with the actual field observations. There are many examples for instance in the IEEE ASIAEX special volume that show several of these features really well. Examples include the squaredoff waves, the broadening of the waves with decreasing water depth, the shape of the broad wave with the shallower slope on the leading edge and the extremely steep back side, even some examples of split waves whose spacing and timing looks similar to the simulated waves. The paper could be strengthened by referring to/comparing more specifically to some of those results. When it looks good, you might as well show it!

*We have added additional comparisons. In addition to the modified text regarding mode-two waves mentioned above we have*

*(a) Added the following text to section 4:*

*“Many of the observations from the ASIAEX program show waves that are broad, with a gently sloping front and steep back, in water of 120 and 85 m depth (Ramp et al (2004), Lynch et al (2004), Duda et al (2004)). These are often trailed by a small number of narrow waves of elevation and square shaped depressions as*

*in our simulations. Figure 3 in (Duda et al, (2004)) shows the presence of waves of elevation in which the thermocline is raised above its rest height in a water depth of 85 m similar to the pedestals generated in our simulations. Ramp et al (2004) show several examples (e.g., 14:00-16:00 GMT on May 7, 15:00:16:00 GMT on May 9, their Figure 6) in which near bottom water is raised well into the water column in waves of elevation trailing a broad wave of depression in water of 120 m depth. In our simulations we start with a single solitary wave in deep water. The shoaling wave fissions into several waves, with at least two well separated solitary waves having been formed by depths of 600–700 m for both bathymetries, with the waves separating at greater depth for bathymetry  $h_0$  which has the more gentle slope. For the steeper bathymetry the waves have reached shallower water before completely separating. In contrast, Lynch et al (2004) and Ramp et al (2004) report that large solitary waves at a depth of 350 m have split into two by the time they reach a depth of 200 m.”*

(b) *Added the following text to section 3.7:*

*“For stratification  $\bar{\rho}_2$  (Fig. 17b) the pycnocline is above the mid-depth on the shelf and solitary waves of depression persist. In this case it can be seen that the leading depression has a steep front (at approximately  $x = 86$  km), in contrast to the other cases. Ultimately a broad square-shaped solitary wave of depression will form. Ramp et al (2004) observed waves of depression at 120 m depth during times when the internal tide had raised the thermocline above the mid-depth (their Figure 6, 18:00 GMT May 13 to 06:00 GMT May 14), some of which have the appearance of broad waves of depression (e.g., between 23:00 and 02:00).”*

2. On a similar but not quite the same note, I think its not quite clear what, if anything, the shoaling has to do with a-waves vs. b-waves. These waves are described in the introduction, and then one might be led to believe that it is the described shoaling mechanism that creates the a-wave packets. Actually, its not, because the a-waves already exist as very clear packets in the deep basin (2500 m water depth) and do not require a shoaling mechanism to create them, they are already there. Thats not to say the work is not relevant: Both large b-waves (which are generally solitary) and the leading wave in a type a-packet (usually the biggest ones) are observed to split and form additional waves as the waves shoal. This only happens for the largest waves generated near the spring tide, but it does happen.

*We did not mean to imply that shoaling creates the a-waves and b-waves and we chose to consider the shoaling of a single solitary wave rather than a packet of waves. Text has been modified by adding*

*“The formation of these wave packets is tied to the generation of the waves in Luzon Strait (Alford et al, (2010), Buijsman et al, 2010).”*

3. Finally, can the authors comment any more on the wave energetics? Is energy conserved, i.e., the energy in the original specified wave equals the sum of the energy in the split-out waves? If not, where is the energy coming from?

*The following text as been added to the of first part of section 3 (before section 3.1):*

*Theoretically energy is conserved as waves shoal if viscosity and diffusion is ignored, however in the simulations the total energy (kinetic plus available potential energy) changes due to numerical error. It can increase slightly in deep water due to numerical diffusion thickening the pycnocline. For case 2 the wave field at  $t = 42$  h (see Figure 4c ) contains 96% of the initial energy, with 90% of the initial energy contained in the wave field on the gently sloping part of the shelf slope ( $x > 90$  km). The leading two solitary waves contain 50% and 16% of the initial energy. At  $t = 50$  h the leading depression contains 42% of the initial energy with 7% of the initial energy now residing in the pedestal between the two leading solitary waves. At  $t = 58$  h only 84% of the initial energy remains. The leading two waves of depression contain 19.9% and 10.9% of the initial wave energy while the pedestal between them has 10.5% of the initial energy. For Case 3 at  $t = 29$  h (Figures 7(c) and 8) the energy in the full wave field is 98.8% of the original energy. The leading wave has about 36% of the original energy, vs 50% for Case 2. The second solitary wave is not cleanly separated from the trailing waves so a precise estimation of its energy is not possible however about 17% of the wave energy lies between 31 and 35 km. Approximately 15% of the wave energy is in reflected waves to the left of the bump ( $x < -15$  km).*

*Additional comments on energy include:*

*Section 3.4 (effect of bumps):*

*“The bump also results in a reduction in wave amplitude, with the leading three waves containing 60% and 71% of the initial wave energy for cases Cases 4 and 4nb. ”*

*Section 3.5:*

*“At the early times shown (panels a, c, e) the leading wave contains 36%, 53% and 75% of the initial wave energy showing a striking increase with the initial wave amplitude.”*

*Smaller stuff:*

4. The title should include something to suggest that these are simulations and not observations

*This is a good idea. The title has been changed to "Two-dimensional numerical simulations of shoaling internal solitary waves at the ASIAEX site in the South China Sea".*

5. Bottom page 2 and top of page 3: Even Zhou and Alford now admit this is wrong! Subsequent work including their own shows its the eastward flow in the strait that pops off the big ones.

*Text has been modified.*

6. Figure 18: (b,c) should be (b,d)

*Figure has been changed and caption has been modified.*

## Response to reviewer #3

1. This study presents a series of 2D, nonhydrostatic model experiments of shoaling internal waves with various amplitudes, model resolutions, 2D bathymetries, rotation, stratification, and viscosity. The simulations are of high resolution of 33 m and 400 layers and show impressive and detailed structure. Novel results are the comparison of the simulations with adiabatic shoaling waves computed using the DJL equation. Can the authors explain what causes the differences between the DJL and numerical model solutions?

*The differences between the DJL and numerical solutions are a consequence of the depth changing sufficiently rapidly that the shoaling waves do not have time to adjust to the changing depth, i.e., the time scale for adjusting towards a DJL solution is longer than the time scale over which the depth changes. This is mentioned in the opening paragraph in section 3.2. We have mentioned this in the summary paragraph of that section.*

2. The paper feels a little long with its 23 figures, and many of the texts accompanying the figures are too descriptive with too much detail. Maybe reduce the text and omit Figures 3a, 4, and 11 (merge with 2), and 21 (merge with 20 and consider one density?).

*The number of figures has been reduced to 19. We have removed one of the panels from figure 3, merged former figures 2 and 11 and eliminated figure 4. In addition legends and colourbars have been added to many figures. Former figures 22 and 23 have been merged by adding the vertical viscosity profile function  $f(z)$  as an extra panel in Figure 23 (now figure 19). Former Figures 20 and 21 have been replaced with new figures comparing the wave fields for all three stratifications with and without rotation at a single time. Former figures 14 and 15 have been*

*merged by showing results at four different times instead of at six different times (new figure 12).*

3. My main criticism is that the justification for this paper is lacking in the introduction. Why is this paper relevant? What does it add to the existing literature that is missing? Including some questions/objectives may improve the focus of this paper. Moreover, it is not always clear why the sensitivity experiments were performed. Maybe mention these reasons in the first lines of each new section? (why use different density profiles? why use different initial depths? why use different viscosities?) The readability is further improved if a brief summary is added at the bottom of each experiment section with the take-home message. This extra text can be offset by omitting some of the descriptive details.

*Further motivation has been added to the introduction:*

*“The large internal solitary waves that shoal onto the Chinese Continental shelf are highly energetic features that have implications for biological productivity and sediment transport (Wang et al 2007, Reeder et al 2011). (St. Laurent 2008) concluded that these waves drive one of the most dissipative coastal regions of the world’s oceans. Thus it is important to understand their shoaling dynamics. While ISWs often appear as packets we have chosen to consider the evolution of a single ISW for simplicity. In this first study we also ignore the important effects of background tidal currents which will modify the shoaling behaviour by introducing time varying currents and stratification. Instead we focus on exploring the sensitivity of the evolution of a single shoaling ISWs for a range of wave amplitudes to the underlying bathymetry, small changes in stratification and the effects of rotation. These simulations are based on observations from the ASI-AEX experimental site (Orr and Mignerey, 2003; Duda et al, 2004; Ramp et al, 2004).”*

*Motivations for some of the sensitivity studies (sections 3.3 (different depths) and 3.7 (different stratifications)) have been added along with some summary take home messages (first part of section 3, section 3.3). We have also provided more motivation for the simulations with viscosity (end of first paragraph of section 3.8):*

- (a) *End of introductory part of section 3 (before section 3.1):*

*In summary, the steep slope between depths of 2250 and 750 m for bathymetry  $h_{15}$  results in significant reflection of incident wave energy. The leading solitary wave in shallow water contains less energy than for the case using bathymetry  $h_0$  which has a gentler slope. For bathymetry  $h_{15}$  two large leading solitary waves are formed in shallow water which are trailed by a train of small amplitude mode-one and higher mode waves that are generated by the interaction of the shoaling wave with the bump. For*

*bathymetry  $h_0$  there are 3–4 solitary waves and the leading solitary wave has about 50% more energy than that in the other case. No trailing mode-one wave train or higher mode waves are evident. When the waves arrive on the shelf large pedestals form which are conjugate to the flow in the leading depression. These waves are much larger than the largest possible solitary wave for the ambient background conditions.*

(b) Section 3.3:

*Intro:*

*For reasons of numerical efficiency it is tempting to truncate the bathymetry and start waves from depths of, say, 1000 m. Here we briefly explore the implications of doing so.*

*Summary:*

*Truncating the deep water depth to 1000 m significantly modifies the fissioning processes resulting in fewer waves, reducing the relative amplitude of the second solitary wave and increasing the distance between the two leading waves.*

(c) Section 3.7: Intro:

*The stratification at the ASIAEX site varied over the course of the field program. Here we consider the sensitivity of the shoaling behaviour to various in stratification over the course of the program. The major difference in our stratifications is the depth of the thermocline which also acts as a proxy for the raising and lowering of the thermocline in response to the internal tides in the region which are not included in our simulations. Ramp et al (2004) report on the influence of the internal tides on the wave forms in shallow water.*

(d) In section 3.8 we have changed the intro to

*In the real world shoaling waves are subject to a no-slip bottom boundary conditions and the effects of boundary layer instabilities as well as diffusion and dissipation related to other physical processes, in particular tidal currents. In order to point out the potential implications of these processes some simulations were done with vertical eddy viscosity/diffusivity of the form*

*and at the end of the introductory paragraph we have added*

*The functional form of the eddy viscosity/diffusivity is ad-hoc. We take the point of view that physically what is important is a mechanism to create boundary layer separation and vortex shedding off the boundary and we do this in a simple way while confining the viscosity/diffusivity to a region close to the bottom boundary. We consider three different values of  $K$  to illustrate of the sensitivity of the results to its value.*

*After listing the three viscosity values we have added “The latter is possibly unrealistically large.”*

4. The figures do not have titles describing experiment cases and times of snapshots, as well as colorbars, legends, transect labels (e.g. Figure 6), etc. It is tiring for the reader to go back and forth between the caption and the figure. I suggest making all figures easier to read by including these things.

*Most of the figures have been modified to include legends and colourbars. We have also added depth values along the upper axis in some of the line plots (e.g., the resolution tests).*

5. P1164, 125. Z&A ref year is 2006!

*Corrected.*

6. P1166, 11. Buijsman and others (see Alford et al 2011) found that westward currents were not the cause of the a and b waves. Simulations indicate eastward currents.

*Text corrected.*

7. P1166, 14. Typo? . . .sloping front have

*Fixed.*

8. P1166, 18. Correct English? KdV extended . . .

*Correct as is.*

9. P1168. L19-15. Omit this detailed description on the bathymetry?

*We have retained the detail as we think it useful to include information on the bathymetric slopes.*

10. P1170. Section 2.4. Is this discussion on alpha relevant for the rest of the paper? Maybe omit?

*This section has been shortened a bit by removing the details about the cubic coefficient  $\alpha_1$ . The discussion of alpha is relevant in so far as it predicts whether or not waves of elevation or depression are formed on the shelf.*

11. P1170, 127. approachED?

*Fixed.*

12. P1172, 13. Feature. At what km? Mark in figure?

*km given in text.*

13. P1172, 17. Same for pedestal. At what km? Mark in figure?

*Location given in text.*

14. P1172, 116-18. Propagating used twice in one sentence.

*We think this sentence is OK as is.*



15. P1172, 125. stronger currents THAN.

*Fixed.*

16. P1173, 16. How did you calculate ISWs?

*Solutions of the DJL equation modified to include background currents (Stastna & Lamb, 2002) were calculated. Text has been modified and references to DJL equation with background currents have been added.*

17. P1174. Section 3.1 and Figure 10d. It seems that there is a large difference in shallow water between  $DX=50$  and 33 m. I wonder if the model simulation has converged with a resolution of 33 m? Can you do a test for  $DX=15$  m, or at least make a statement about the model convergence in this section?

*We did not mean to suggest the simulations had converged. We have done an additional simulation using a horizontal resolution of 16 m and a new panel has been added to the figure comparing results from different resolutions. A comment about convergence has been added to the text. The results have converged well up to about the time the leading waves reach a depth of 140 m. For the 16 m resolution case the back of the leading depression is steeper but better resolved than in the 33 m resolution case (7–8 grid points vs 4–5). After breaking commences they become quite different in detail. The front part of the leading depression is the same but the steep backs drift apart in the two cases. At  $t = 42$  h (time of last panel in original version of the paper) the steep back of the leading depression in the 33 m resolution case lags that in the 50 m case by a bit more than 600 m and leads that in the 16 m resolution case by a bit more than 400 m. That is, as the resolution increases the leading depression increases in length and there is more energy in the leading depression. This could be a consequence of numerical dissipation which increases as the resolution decreases. It is clear that results have not converged even at a resolution of 16 m.*

18. P1177. Section 3.2. It is not explained in this section what causes the deviation between the DJL solutions and the simulations. Is it the nonlinear advection terms in the momentum equation? Wave breaking? How does the supercriticality (=slope angle over beam angle) of the slope affect these differences? Do the simulations become exactly the same as the DJL simulations when a subcritical slope is used (that would be a fun experiment)? The criticality of the slope is nowhere discussed in the paper and its relevance for the simulations and evolution of the solitary wave (see Klymak et al 2011, JPO)?

*As pointed out above, the deviation is a consequence of the short time scale over which the shoaling waves experience a depth change vs the time scale for it to adjust to its new depth. We do not know what terms are responsible but it is not a consequence of wave breaking as wave breaking does not occur until depths of less than 200 m are reached. The concept of subcritical or supercritical slopes is normally applied to waves with a well defined frequency (e.g., the internal tide, as done by Klymak et al). For a shoaling solitary wave the flow along the bottom experiences a single short downward flow followed by a single short upward flow. We estimated a frequency  $\omega = ck$  where  $c$  is the estimated propagation*

*speed of the solitary wave and  $k = 2\pi/\lambda$  where  $\lambda$  was taken as four times the length of the front half of the wave, defined as the distance from the crest to the point where the surface current was 5% of its peak value. Using this frequency we estimate that the slope is always subcritical and that along much of the slope  $\omega^2$  is less than  $N^2$ . The closest the slope comes to being critical (apart from a very narrow region when  $N^2 - \omega^2$  changes sign) is above the left side of the bump for bathymetry  $h_{15}$  where the ray slopes are estimated to be 4, 3 and 2 times the bathymetric slope. This of course is sensitive to the choice of the wave width which determines the frequency  $\omega$ . We think this approach to predicting fissioning and/or wave breaking is best left for a more detailed study.*

19. P1177, 112. Typo: long small amplitude shelf?

*added a comma after “long”*

20. P1178, 110. energy increases. Is this energy increase for the same wave as it shoals? Where is this energy coming from? This somewhat contrasts with the statement on 120. Please explain/rewrite.

*These statements are not for shoaling waves. The DJL equation is solved for a specified APE. As the water depth decreases the total energy of the solitary waves for fixed APE increases at first because the kinetic energy of the waves increases (i.e., the ratio KE/APE increases). There is a water depth at which the kinetic, and hence total, energy has its maximum value. As the water depth decreases beyond that point the total energy of solitary waves for fixed APE decreases. We have modified the first sentence (now the start of a paragraph) to read “As the water depth decreases from 3000 m with the APE fixed the total wave energy increases due to the increasing KE/APE ratio, .....”.*

21. P1180, 16. increase more slowly What causes this difference?

*We do not know why the currents would adjust more slowly than the amplitude does.*

22. p1186, section 3.7. What is the relevance of this section to the reader? Why not use summer and winter stratifications? Remove/shorten this section?

*The stratification observed in the summer does exhibit some variability and our goal was to explore the sensitivity of the shoaling behaviour to this variability. Clearly large differences would be expected if a winter stratification was used. We have replaced the figures used to illustrate this variability and modified the text accordingly. See in particular the introduction to section 3.7 quoted above.*

23. P1190, 128. Typo? as THE shoal

*Fixed.*

Manuscript prepared for Nonlin. Processes Geophys. Discuss.  
with version 2014/07/29 7.12 Copernicus papers of the L<sup>A</sup>T<sub>E</sub>X class copernicus.cls.  
Date: 29 January 2015

# **Shoaling** Two-dimensional numerical simulations of shoaling internal solitary waves at the ASIAEX site in the South China Sea

**K. G. Lamb<sup>1</sup> and A. Warn-Varnas<sup>2,\*</sup>**

<sup>1</sup>Department of Applied Mathematics, University of Waterloo, Waterloo, Ontario, N2L 3G1, Canada

<sup>2</sup>Naval Research Laboratory, Stennis Space Center, MS 39539, USA

\*retired

Correspondence to: K. G. Lamb (kglamb@uwaterloo.ca)

## Abstract

The interaction of barotropic tides with Luzon Strait topography generates ~~westward propagating internal bores and solitary waves trains~~ some of the world's largest internal solitary waves which eventually shoal and dissipate on the western side of the north South China Sea. Two-dimensional numerical simulations of ~~this shoaling process~~ the shoaling of a single internal solitary wave at the site of the Asian Seas International Acoustic Experiment (~~ASIAEX~~) have been undertaken in order to investigate the sensitivity of the shoaling process to the stratification and the underlying bathymetry, and to explore the influence of rotation. ~~A range of wave amplitudes are considered. Comparisons with adiabatic shoaling waves are also made and the potential impact of~~ The bulk of the simulations are inviscid however exploratory simulations using a vertical eddy-viscosity confined to a near bottom layer, along with a non-slip boundary condition are briefly explored. On the slope secondary solitary waves and mode-two wave packets are generated which propagate towards the shelf. Comparisons with observations made during the ASIAEX experiment are made. ~~no-slip boundary condition, suggest that viscous effects may become important in water shallower than about 200 m. A shoaling solitary wave fissions into several waves. At depths of 200-300 m the front of the leading waves become nearly parallel to the bottom and develop a very steep back as has been observed. The leading waves are followed by waves of elevation (pedestals) that are conjugate to the waves of depression ahead and behind them. Horizontal resolutions of at least 50 m are required to simulate these well. Wave breaking was found to occur behind the second or third of the leading solitary waves, never at the back of the leading wave. Comparisons of the shoaling of waves started at depths of 1000 and 3000 m show significant differences and the shoaling waves can be significantly non-adiabatic even at depths greater than 2000 m. When waves reach a depth of 200 m their amplitudes can be more than 50% larger than the largest possible solitary wave at that depth. The shoaling behaviour is sensitive to the presence of small scale features in the bathymetry: a 200 m high bump at 700 m depth can result in the generation of many mode-two waves and of higher mode waves. Sensitivity to the~~

stratification is considered by using three stratifications based on summer observations. They primarily differ in the depth of the thermocline. The generation of mode-two waves and the behaviour of the waves in shallow water is sensitive to this depth. Rotation affects the shoaling waves by reducing the amplitude of the leading waves via the radiation of long trailing inertia-gravity waves. The nonlinear-dispersive evolution of these inertia-gravity waves results in the formation of secondary mode-one wave packets.

## 1 Introduction

In the South China Sea (SCS) large internal solitary-like waves (ISWs) are frequently observed, both remotely via Synthetic Aperture Radar (SAR) and in situ observations (Liu et al., 1998; Ramp et al., 2004; Klymak et al., 2006; Farmer et al., 2009; Li and Farmer, 2011). Analysis of SAR surface signatures, and time series of current and temperature data at moorings, indicate that the ISWs are generated by barotropic tidal motion over the large sills in Luzon Strait and on the slope region of the northern boundary of the SCS (Liu et al., 1998; Hsu and Liu, 2000) (Liu et al., 1998; Hsu and Liu, 2000; Alford et al., 2010). Depressions generated in Luzon Strait propagate westwards across the deep South China Sea basin, where depths can exceed 4000 m, to the Asian Seas International Acoustic Experiment (ASIAEX) experimental site on the Chinese continental shelf. Nonlinear effects steepen these depressions until they disintegrate into ISWs of large amplitude, through frequency and amplitude dispersion. Zhao and Alford (2006) related the ISWs observed near Dongsha Island to tidal currents passing through Luzon Strait, finding that westward flow through the strait was responsible for the generation of the ISW packets however more recent studies have shown that eastwards currents are responsible for generating the large westward propagating solitary waves (Buijsman et al., 2010).

Li and Farmer (2011) reported deep basin ISW amplitudes as large as 150 m with typical values being around 50 m. In situ measurements in the deep basin by Klymak et al. (2006) show ISWs with amplitudes as large as 170 m and phase speeds of  $2.9 \text{ m s}^{-1}$ . During the joint Variations Around the Northern South China Sea (VANS) and Windy Island Soliton

Experiment (WISE) (Yang et al., 2009), ISWs with amplitudes of up to 220 m and phase speeds of around  $3.4 \text{ m s}^{-1}$  were observed (Ramp, private communication) ~~were observed~~. These measured amplitudes and phase speeds are among the largest observed anywhere, surpassing observed amplitudes of 90 m and phase speeds of  $1.8 \text{ m s}^{-1}$  in the Andaman and Sulu Seas (Osborne and Burch, 1980; Apel et al., 1985). Because of the large amplitudes of these waves they have been the subject of many observational and numerical investigations. The dynamics of ISWs in the northern SCS was recently reviewed by Guo and Chen (2014).

Several numerical studies of ISW generation by tidal flow over the ridges in Luzon Strait have been conducted (Niwa and Hibiya, 2001, 2004; Warn-Varnas et al., 2010; Buijsman et al., 2010) elucidating the generation of ISWs in Luzon Strait and their subsequent westward propagation in the South China Sea. The structure of ISW wave trains in the SCS is variable with large amplitude wave trains separated by small amplitude wave trains (Ramp et al., 2004; Warn-Varnas et al., 2010; Buijsman et al., 2010; Vlasenko et al., 2012). Ramp et al. (2004) separated the wave packets observed at the ASIAEX site into *a* waves and *b* waves. The *a* waves arrived at regular 24 h intervals and were rank ordered, with the largest wave leading the wave packet. The weaker *b* waves were separated by approximately 25 h and were more irregular, with the largest wave usually in the middle of the packet. The formation of these wave packets is tied to the generation of the waves in Luzon Strait (Alford et al., 2010; Buijsman et al., 2010) .

During the ASIAEX experiment, intensive measurements of shoaling ISW trains over the continental shelf off China were undertaken (Lynch et al., 2004; Duda et al., 2004; Orr and Mignerey, 2003; Ramp et al., 2004). Ramp et al. (2004) reported on observations from a series of moorings spanning depths of 350 to 72 m. At 350 m depth wave amplitudes ranged from 29 to 142 m (based on the displacement of the  $24^\circ$  isotherm). Their observations illustrated the evolution of these waves as they shoaled. At 350 m depth the waves were fairly symmetric. By the time they reached a depth of 200 m they had usually deformed significantly with a gently sloping front ~~have~~ and a much steeper rear. Orr and Mignerey (2003) tracked a shoaling solitary wave train with a towed conductivity, tem-

perature, and depth sensor (CTD), observing the evolution of shoaling ISW trains from waves of depression to waves of elevation. Mode-two solitary-like waves were observed the ASIAEX experiment (Orr and Mignerey, 2003) but not reported on in detail. Observations of a mode-two ISW made during a pilot study for the ASIAEX experiment were reported on in Yang et al. (2004). Many mode-two solitary-like waves were observed at 350 m depth in a nearby region during the joint VANS/WISE experiments (Yang et al., 2009, 2010). They appear to have been generated by shoaling mode-one ISWs.

Liu et al. (1998) demonstrated, with a two-layer Gardner equation ~~(Kortweg-deVries extended to include a cubic nonlinear term) model that~~ model that includes cubic nonlinearity, that ISW depressions are transformed into a train of ISWs of elevation as they propagate over sloping topography into shallower water ~~where the upper layer is thinner than the lower layer, as did Orr and Mignerey (2003) who based their simulations on observations from the ASIAEX site.~~ Recently Grimshaw et al. (2014) used the Ostrovsky equation to investigate the effects of rotation on the evolution of shoaling solitary waves. They too included a cubic nonlinear term. Their simulations were based on bathymetry and continuous stratifications observed in the South China Sea. They found that a significant consequence of rotation was the formation of a secondary trailing wave packet associated with nonlinear steepening of the radiated inertia gravity waves. They also conducted fully nonlinear simulations using the MITgcm. Vlasenko and Stashchuk (2007) studied three-dimensional shoaling in the Andaman Sea with a fully nonlinear nonhydrostatic numerical model using a continuous stratification. Results showed the transformation of ISWs of depression to waves of elevation as well as refraction effects. ~~Orr and Mignerey (2003) modeled a single shoaling soliton with the Gardner equation and showed a change from depression to elevation over their measurement slope.~~

~~The vast majority of observed nonlinear internal waves in the South China Sea are mode-one waves however several observations of mode-two waves have been made. During VANS/WISE mode-two waves were observed on the Chinese continental slope at 350 depth where they appear to have been generated by shoaling mode-one ISWs (Yang et al., 2009, 2010).~~

The breaking of solitary waves travelling up slope has been addressed by several researchers. Helfrich and Melville (1986) and Helfrich (1992) considered the breaking criteria for a two-layered system. Vlasenko and Hutter (2002) performed simulations, in a continuously stratified fluid, of breaking solitary waves on slope-shelf topography and determined a parametrization for the location of wave breaking for stratifications and bathymetry based on observations in the Andaman and Sulu Seas.

~~In this study modeling of a shoaling solitary wave train is undertaken at the~~ The large internal solitary waves that shoal onto the Chinese Continental shelf are highly energetic features that have implications for biological productivity and sediment transport (Wang et al., 2007; Reeder et al., 2011) . St. Laurent (2008) concluded that these waves drive one of the most dissipative coastal regions of the world's oceans. Thus it is important to understand their shoaling dynamics. While ISWs often appear as packets we have chosen to consider the evolution of a single ISW for simplicity. In this first study we also ignore the important effects of background tidal currents which will modify the shoaling behaviour by introducing time varying currents and stratification. Instead we focus on exploring the sensitivity of the evolution of a single shoaling ISWs for a range of wave amplitudes to the underlying bathymetry, small changes in stratification and the effects of rotation. These simulations are based on observations from the ASIAEX experimental site (Orr and Mignerey, 2003; Duda et al., 2004; Ramp et al., 2004).

The model, bathymetries and stratifications used in this study is described in Sect. 2. Results of the simulations are presented in Sect. 3 where sensitivity to the bathymetry, stratification, rotational effects and the potential implications of viscosity are considered. We also present results from resolutions tests and consider the adiabaticity of the shoaling waves. Comparisons with observations from the ASIAEX and conclusions are presented in Sect. 4.



## 2 Modelling

### 2.1 Numerical model

The two-dimensional fully nonhydrostatic Internal Gravity Wave model (Lamb, 1994, 2007) is used in this study of shoaling ISWs. Flow in the along shelf  $y$ -direction is included but the flow is independent of  $y$ . The model uses the rigid-lid, traditional  $f$ -plane, Boussinesq and incompressible flow approximations. The governing equations are

$$\mathbf{u}_t + \mathbf{u} \cdot \nabla \mathbf{u} - f \mathbf{u} \times \hat{k} = -\frac{1}{\rho_0} \nabla p - \frac{\rho}{\rho_0} g \hat{k} + \nabla \cdot (\nu \nabla \mathbf{u}), \quad (1a)$$

$$\rho_t + \mathbf{u} \cdot \nabla \rho = \nabla \cdot (\nu_T \hat{k} \nabla \rho), \quad (1b)$$

$$\nabla \cdot \mathbf{u} = 0, \quad (1c)$$

where  $z$  is the vertical coordinate,  $(x, y)$  are the horizontal coordinates directed across and along the topography,  $\mathbf{u} = (u, v, w)$  is the velocity field with components in the  $(x, y, z)$  directions,  $\hat{k}$  is the unit vector in the  $z$ -direction,  $\rho$  is the density,  $\rho_0$  is the reference density, and  $p$  is the pressure.  $\nabla$  is the 3-D vector gradient operator, however all fields are independent of  $y$ . The subscript  $t$  denotes differentiation with respect to time. The gravitational acceleration is  $g = 9.81 \text{ m s}^{-2}$  and for simulations including rotational effects the Coriolis parameter is  $f = 5.33 \times 10^{-5} \text{ s}^{-1}$  corresponding to a latitude of  $21.5^\circ$  N.  $\nu$  and  $\nu_T \hat{k}$  are a spatially varying viscosity and diffusivity. ~~Most, however for most of our simulations do not use explicit viscosity and diffusion terms, we return to this later~~ these are set to zero. The model uses flux limiting which acts to control the overturns that occur in the simulations. In the ocean strong mixing can occur. A proper account of this important problem is left for future work. Before the equations are solved, they are transformed to a terrain following coordinate system (sigma-coordinates) in the vertical, which leads to higher vertical resolution in shallower water. The equations are solved over a domain bounded below by the topography and a rigid lid at  $z = 0$ . Except for some test cases the simulations used

$J = 200$  grid cells in the vertical with the height of the grid cells varying in the deep water to improve resolution across the thermocline. The model uses a variable time step to satisfy a CFL condition.

## 2.2 Bathymetry

Twenty five sample shelf break bathymetries in the area of ASIAEX (see red square in Fig. 1), as extracted from the Digital Bathymetry 2 min resolution (DB2) data base, are shown by the grey curves in Fig. 2. They contain many small deviations from their average indicative of a large number of small-scale bathymetric features which vary in the along shelf direction. The solid and dotted black curves in Fig. 2a show the two base bathymetries used in our simulations, about which some variations for sensitivity studies were conducted. These bathymetries are compared with two measured bathymetries in Fig. 2b and c and are referred to as  $h_0$  (transect 0) and  $h_{15}$  (transect 15) bathymetries respectively. These bathymetries were chosen because they are representative of transects with the smallest and largest slopes between depths of about 500 and 2500 m.

Bathymetry  $h_0$  has a uniform depth of 3000 m before it starts to rise gently with a slope of 0.005. The slope steepens to 0.015 at a depth of 2700 m, steepens again to 0.03 at a depth of 1950 m, decreases to 0.004 at a depth of 750 m and then levels off at a depth of 80 m. There is a bump of about 200 m amplitude at a depth of about 2100 m. The water depth at the top of the bump is about 1900 m. The depth then increases to about 2000 m after which it decreases monotonically. Bathymetry  $h_{15}$  also starts with a gentle slope of 0.005. It steepens to 0.01 at a depth of 2700 m and steepens again to 0.05 for depths between 2250 and 750 m. This is the steepest slope for either bathymetry. The slope then decreases to 0.007 until a depth of 80 m is reached. ~~This is 75 steeper than the final part of the slope in bathymetry  $h_0$ . Superimposed on these slopes is Bathymetry  $h_{15}$  has~~ a 10 km long bump with a height of approximately 200 m high bump at a depth of about 700 m separating the 0.05 and 0.007 slopes. The depth at the top of the bump is about 480 m. Some simulations were done with a modified topography with this feature removed (see Fig. 2c).

In the simulations the grid is arranged so that the shelf starts at approximately  $x = 80$  km. The shelf slope for bathymetry  $h_0$  lies between  $-250$  and  $80$  km while that for  $h_{15}$  lies between about  $x = -150$  and  $80$  km.

## 2.3 Stratification and model initialization

Three different stratifications have been considered (Fig. 3). ~~Figure 3a shows the density profiles over the full depth, Fig. 3b shows the upper 500 and Fig. 3c shows the profiles in the upper 400 along with two observed stratifications. The buoyancy frequency profiles are shown in Fig. 3d.~~ Four stratifications are shown in the first two panels: our base stratification  $\bar{\rho}_b(z)$ , two fits to observed stratifications measured at the ASIAEX site (Orr and Mignerey, 2003),  $\bar{\rho}_1$  and  $\bar{\rho}_2$ , and  $\bar{\rho}_w$ , which is the density west of Luzon Strait used in Warn-Varnas et al. (2010). Profiles  $\bar{\rho}_1(z)$  and  $\bar{\rho}_2(z)$  are fits to two stratifications observed during the ASIAEX ~~experimental site experiment~~. The observed profiles are included in Fig. ~~3e3b~~. These profiles were chosen because they have the thermocline at the lower and upper range of observed thermocline depths. ~~Significant differences between  $\bar{\rho}_w$  and  $\bar{\rho}_b$  occur in the top 200. Stratification  $\bar{\rho}_b$  has a sharp pycnocline at around 50 depth while  $\bar{\rho}_w$  has a broader pycnocline between depths of 50 and 100.~~

We ~~initialize~~ initialize our simulations with internal solitary wave solutions of the governing equations obtained by solving the Dubreil–Jacotin–Long (DJL) equation (Lamb, 2002). The DJL solver provides an initial ISW with a prescribed available potential energy (APE). This procedure does not take rotational effects into account, as exact ISWs do not exist on the  $f$ -plane. In simulations that include rotational effects, appropriate to the latitude of the South China Sea, the initial waves undergo a continual adjustment which results in a continual loss of energy from the leading ISW (Helfrich, 2007; Grimshaw et al., 2014). Because of this the shoaling behaviour will depend on the initial location of the ISW. We do not consider this. The initial waves are placed in the deep water. Because of the different lengths of the shelf slopes the initial location depends on the bathymetry: for bathymetries  $h_0$  and  $h_{15}$  the waves are started at  $x = -280$  and  $-200$  km respectively.

We have used waves with several different amplitudes based on observed amplitudes (Ramp et al., 2004). The energies and wave amplitudes for several different initial waves are provided in Table 1.

## 2.4 Weakly-nonlinear theory and conjugate flow amplitudes

Weakly-nonlinear theory is often used to approximate observed internal solitary waves and it provides some insight into the expected behaviour of shoaling waves. Including cubic nonlinearity and ignoring damping and rotational effects, internal solitary waves in a fluid of constant depth can be modeled with the Gardner (or extended KdV) equation

$$\eta_t + c_0\eta_x + \alpha\eta\eta_x + \alpha_1\eta^2\eta_x + \beta\eta_{xxx} = 0. \quad (2)$$

~~Ignoring the cubic nonlinear term is ignored (i.e.  $\alpha_1 = 0$ ) results in the KdV equation. It. The KdV equation predicts solitary waves of depression when  $\alpha < 0$  and solitary waves of elevation when  $\alpha > 0$ . For our base stratification  $\alpha < 0$  for depths greater than Stratifications  $\bar{\rho}_b$  and  $\bar{\rho}_1$  have critical points, locations where  $\alpha$  changes sign, at depths of about 91.8 and 120.0 m and positive in shallower depths respectively: in greater depths ISWs are waves of depression while in shallower depths, in particular on the shelf, ISWs are waves of elevation. Thus for these two stratifications shoaling waves pass through a critical point on their way to the shelf which has significant implications for their evolution. Stratification  $\bar{\rho}_2$ , with its higher pycnocline, does not have a critical point for the chosen shelf depth of 80 m.~~

When  $\alpha_1 < 0$  solitary wave solutions of the Gardner equation have a limiting amplitude of  $-\alpha/\alpha_1$  while for  $\alpha_1 > 0$  solitary waves of depression and elevation exist. When  $\alpha < 0$  waves of depression with any amplitude exist while waves of elevation exist with amplitudes greater than the minimum amplitude of  $-2\alpha/\alpha_1$ . The opposite is the case when  $\alpha > 0$ . with unbounded amplitudes exist (Grimshaw et al., 2004). Using  $\alpha_1$  to predict the existence of solitary waves with both polarities is problematic because  $\alpha_1$  is not uniquely determined (Lamb and Yan, 1996). Choosing  $\alpha_1$  so that the second-order vertical structure function

for the isopycnal displacement is zero at the depth where the leading-order eigenfunction has its maximum is a common choice (Grimshaw et al., 2002). This choice for selecting  $\alpha_1$  predicts that solitary waves of either polarity exist in depths greater than 235 m using our base stratification. In shallower water it predicts that only waves of one polarity exist.

Fully nonlinear ISWs generally have limiting amplitudes. As this amplitude is ~~approach~~ approached they broaden and become horizontally uniform in their centre. The flow state in the centre of these flat-crested waves is called a conjugate flow. We computed conjugate flow solutions for depths between 50 and 400 m which provide the limiting asymptotic amplitude, propagation speeds and maximal currents for solitary waves (~~Lamb and Wan, 1998~~) as the wave energy goes to infinity (Lamb and Wan, 1998). The amplitudes of these solutions for the base stratification  $\bar{\rho}_b$  ~~are shown in Fig. ??~~. ~~Again, only varied approximately linearly from -160 m to 20 m as the depth decreased from 400 to 60 m. Only~~ single solutions were found (~~which vary almost linearly with depth~~). ~~These solutions have with~~ the polarity predicted by the KdV equation.

~~Stratifications  $\bar{\rho}_b$  and  $\bar{\rho}_1$  have critical points, locations where  $\alpha$  changes sign, at depths of about 91.8 and 120.0 respectively: in greater depths ISWs are waves of depression while in shallower depths, in particular on the shelf, ISWs are waves of elevation. Thus for these two stratifications shoaling waves pass through a critical point on their way to the shelf which has significant implications for their evolution. Stratification  $\bar{\rho}_2$ , with its higher pycnocline, does not have a critical point.~~

### 3 Results

~~We have used waves with several different amplitudes based on observed amplitudes (Ramp et al., 2004). The energies and wave amplitudes for several different initial waves are provided in Table 1~~ Table 2 provides information on the simulations that have been undertaken using a deep water depth of 3000 m. Information provided includes the stratification used, the initial wave energy and wave amplitude and the bathymetry used.

## 4 Results

We begin by showing results for two simulations using an initial wave of amplitude ~~45.545.4 m with each of the~~ (APE 100 MJ m<sup>-1</sup>), ~~the base stratification  $\bar{\rho}_b$  and the two bathymetries~~ (Cases 2 and 3). Following this we explore sensitivity to resolution before discussing more fully the complete set of simulations.

Figure 4 shows results from ~~a simulation using bathymetry  $h_0$  and the base stratification  $\bar{\rho}_b$~~  (Case 2). ~~small initial wave of amplitude 45.4 is used in water 3000 deep (APE 50).~~ ~~Figure 5a Case 2. Fig. 4a~~ shows the full continental slope and the initial wave which is barely visible at  $x = -280$  km. After 25 h the leading wave is at  $x = -64$  km where the water depth is about 650 m (Fig. 4b). A second solitary wave is visible approximately 15 km behind the leading wave. At  $t = 42$  h (Fig. 4c) the leading wave, approximately 1.5 km in length, has reached a depth of 250 m at  $x = 37$  km. Three solitary waves are now visible. By  $t = 50$  h (Fig. 4d) the leading wave has significantly deformed. It is now about 3 km long and spans water depths of 130 to 140 m. The slope of the wave front is less that it was at  $t = 42$  h and in the centre of the wave the slope of the thermocline is greatly reduced, being almost parallel with the bottom (~~between 65.5 and 67.5 km~~). This is a well know feature of shoaling waves when the thermocline is close to the bottom (Vlasenko and Hutter, 2002; Orr and Mignerey, 2003; Lamb and Nguyen, 2009). The rear of the wave is much steeper and behind the leading depression the thermocline has been raised above its equilibrium position ( ~~$x = 66$  km~~). This we refer to as the wave pedestal. There are now three distinct waves of depression trailing the leading wave. As the wave continues to shoal and passes beyond the critical point at 91 m depth (Fig. ~~5e 4e~~), the front part of the leading depression becomes very long with a very shallow slope. On the shelf solitary waves of depression in the ambient stratification do not exist so the leading depression gradually fades away losing energy to the trailing waves. The steep back of the wave never overturns and the second solitary wave, which has now propagated into the pedestal behind the leading wave, has the form of a square wave with the centre of the wave parallel to the bottom separating a very steep front and back (Fig. 5e). This wave is approximately at the critical point of the back-

ground stratification but it is propagating on the wave pedestal trailing the leading wave and this is the environment it propagates in. This environment consists of a background sheared flow with positive vorticity ( $u_z > 0$ ) and a modified stratification. By  $t = 66$  h the waves are on the shelf. Breaking has commenced behind the third depression.

Figure 5 shows a close up of the ~~wave field and~~ leading waves and the wave breaking at  $t = 66$  h. Vertical profiles of the horizontal velocity and density in the wave depressions and wave pedestals at the locations indicated by the vertical dashed lines are shown in Fig. 6a and b. In the two wave depressions (profiles at  $x = 94$  and  $91$  km) the horizontal velocities are similar. The second pedestal (at  $x = 89$  km) has stronger currents ~~that than~~ the first does ( $x = 92$  km). Furthermore in the second pedestal the current at the bottom has a bulge with the maximum current of about  $0.5 \text{ m s}^{-1}$  occurring about  $5$  m above the bottom. This is equal to the estimated propagation speed of the rear of the second pedestal. The density profiles (Fig. 7b6b) show that in the second pedestal fluid in the lower  $22$  m is denser than the fluid ahead of the wave, a consequence of advection of dense water onto the shelf. This denser fluid can also be seen in Fig. 5 where a thin layer of this denser fluid can be seen to extend along the bottom into the depression ahead. The two pedestals have amplitudes of over  $20$  m which is well in excess of the conjugate flow amplitude (~~limiting amplitude for internal solitary waves~~) of  $7.7$  m for the ambient stratification on the shelf. We calculated ISWs of depression ~~using background density and velocity profiles extracted from the first for a~~ background field given by conditions in the pedestal at  $x = 92$  km by solving a version of the DJL equation that includes background currents (Stastna and Lamb, 2002; Lamb, 2003). The computed waves had a maximum amplitude of  $36.6$  m. At this amplitude waves are flat crested similar to the second depression centred at  $90.5$  km in Fig. 5. The flow in the centre of the computed solitary wave is the conjugate flow corresponding to the background conditions. Figure 6c and d compares the vertical profiles of the horizontal velocity and density field of the conjugate flow in the centre of the computed ISW with the vertical profiles from the second depression in the simulation (from  $x = 91$  km). The two sets of profiles are virtually identical except near the bottom showing that the second square-shaped wave of depression is a flat-crested solitary wave riding on the background flow providing by the

wave pedestal just ahead of it. As the velocity and density profiles in the second depression are very similar to those at the back of the leading depression (before the steep rear of the wave) at  $x = 94$  km, the flow in the first pedestal is conjugate to the flow in the depression immediately ahead of it. The waves on the shelf have not however achieved a steady state. The amplitudes of the leading depression slowly decays (solitary waves of depression do not exist on the shelf) and as it does the amplitude of the [pedestal-trailing-trailing pedestal](#) also decays as do the waves behind it.

Figure 7 shows results from a simulation using bathymetry  $h_{15}$  with the same initial wave (Case 3), now at  $x = -200$  km. The results are similar to those using bathymetry  $h_0$  but there are some differences. In both cases the shoaling wave fissions into two large solitary waves trailed by a number of smaller waves. For bathymetry  $h_0$  the trailing waves [consists consist](#) largely of a couple of smaller solitary waves (at  $x \approx 55$  km in Fig. 4d) whereas for the steeper bathymetry  $h_{15}$  the trailing waves are smaller and there are many more of them (e.g. Fig. 7c). The shelf slope for bathymetry  $h_{15}$  is shorter than that for bathymetry  $h_0$  which is likely responsible for the two leading waves being closer together when bathymetry  $h_{15}$  is used. As a consequence, when the leading waves arrive on the shelf the wave pedestal between the leading and second waves of depression is much shorter for bathymetry  $h_{15}$  (500 m vs. 1500 m). In addition to the differences in the steepness of the shelf slope bathymetry  $h_{15}$  has a bump at a depth of about 700 m, much shallower than the bump in bathymetry  $h_0$ . This bump modifies the wave field resulting in the generation of higher mode waves (Fig. 7b) as can be seen by the internal wave beam sloping up from the bump. A zoom in of the higher-mode waves at  $t = 29$  h (same time shown in Fig. [8e7c](#)) is shown in Fig. 8. [The two dashed white boxes contain mode-two waves \(the second box also includes higher mode waves\)](#). Downwelling behind the bump after the wave has passed over it can be seen at  $x \approx -15$  which can in some cases result in larger vertical excursions than in the leading wave. Breaking behind the shoaling waves commences earlier for the steeper bathymetry (compare Figs. 4e and 7e). [Significant wave reflection also occurs in this case due to the steeper bathymetry.](#)



Theoretically energy is conserved as waves shoal if viscosity and diffusion is ignored, however in the simulations the total energy (kinetic plus available potential energy) changes due to numerical error. It can increase slightly in deep water due to numerical diffusion thickening the pycnocline. For case 2 the wave field at  $t = 42$  h (see Figure 4c ) contains 96% of the initial energy, with 90% of the initial energy contained in the wave field on the gently sloping part of the shelf slope ( $x > 90$  km). The leading two solitary waves contain 50% and 16% of the initial energy. At  $t = 50$  h the leading depression contains 42% of the initial energy with 7% of the initial energy now residing in the pedestal between the two leading solitary waves. At  $t = 58$  h only 84% of the initial energy remains. The leading two waves of depression contain 19.9% and 10.9% of the initial wave energy while the pedestal between them has 10.5% of the initial energy.

For Case 3 at  $t = 29$  h (Figures 7(c) and 8) the energy in the full wave field is 98.8% of the original energy. The leading wave has about 36% of the original energy, vs 50% for Case 2. The second solitary wave is not cleanly separated from the trailing waves so a precise estimation of its energy is not possible however about 17% of the wave energy lies between 31 and 35 km. Approximately 15% of the wave energy is in reflected waves to the left of the bump ( $x < -15$  km).

In summary, the steep slope between depths of 2250 and 750 m for bathymetry  $h_{15}$  results in significant reflection of incident wave energy. The leading solitary wave in shallow water contains less energy than for the case using bathymetry  $h_0$  which has a gentler slope. For bathymetry  $h_{15}$  two large leading solitary waves are formed in shallow water which are trailed by a train of small amplitude mode-one and higher mode waves that are generated by the interaction of the shoaling wave with the bump. For bathymetry  $h_0$  there are 3–4 solitary waves and the leading solitary wave has about 50% more energy than that in the other case. No trailing mode-one wave train or higher mode waves are evident. When the waves arrive on the shelf large pedestals form which are conjugate to the flow in the leading depression. These waves are much larger than the largest possible solitary wave for the ambient background conditions.

### 3.1 Resolution

It is important to have high enough resolution to adequately resolve solitary waves as they shoal. If the resolution is too low unphysical solitary-like waves can be simulated due to a balance between nonlinearity and numerical dispersion (Hodges et al., 2006; Vitousek and Fringer, 2011). Vitousek and Fringer (2011) considered waves propagating in a 2000 m deep domain using a stratification based on observations in the South China Sea and found that resolutions coarser than about 250 m resulted in waves that were two too wide.

We have performed a number of resolution tests. In the first series of tests the horizontal resolution was varied ( $\Delta x = 250, 100, 50$  and  $33$  and  $16$  m). In the first set an initial wave of amplitude 45 m shoaled from a depth of 3000 m using bathymetry  $h_{15}$ . The ~~waves were started at  $x = -200$ . The~~ maximum time steps were 12.5, 5.0, 2.5, 2.5 and 2.5 s respectively and a uniform vertical resolution of  $J = 200$  was used. ~~Results from the case with  $\Delta x = 33$  were shown in Fig. 7. For the highest resolution case the time step decreased to approximately 1.4 s by the time the wave reached the shelf.~~ Increasing the time step to 5.0 s in the  $\Delta x = 50$  m simulation resulted in negligible differences. After traveling over 120 km to a depth of 2500 m the amplitudes in all four five cases varied by about 2% with the wave amplitude increasing as the resolution increased. By the time the waves had travelled 180 km to a depth of 800 m, just before the bump, the solitary wave in the  $\Delta x = 250$  m simulation was about 5% smaller than that in the highest resolution case. After this stage the solutions diverged more rapidly.

Figure 9 compares the surface currents  $u(x, 0, t)$  at four different times when the leading wave is in water depths of 600, 395, 180 and 85 m. ~~The first two panels compare results from the three coarsest resolutions, the results from the two finest resolved cases being nearly identical at these depths. At 180 depth we only show results from the three finest resolutions.~~ By the time the waves have reached a depth of 600 m (Fig. 10a) the leading wave has begun fissioning into several waves. The wave in the 250 m resolution case is significantly smaller than those in the other simulations. ~~By the time the wave has reached a depth of~~ while the wave in the 100 m resolution cases is almost indistinguishable from the high resolution

case. At 395 m depth (Fig. 10b) the amplitude of the leading wave in the 250 m resolution case is grossly underestimated and has the form of a small undular bore. In contrast in the higher resolution simulations two large leading solitary waves have emerged trailed by a train of smaller waves. The amplitude of the leading wave in the 100 m resolution simulation is now about 87 % that of the highest resolution case. ~~The result from the 50 resolution simulation is indistinguishable from the 33 resolution case at 600 and 395 depths. By the time the waves have reached~~ At a depth of 180 m (Fig. 10c) the amplitude of the leading wave in the 100 m simulation ~~has continued to decay relative to the higher resolution simulation. It now has an amplitude~~ is approximately 77% of that in the 33 m resolution case. ~~Results from the 50 and 33 resolution cases can now be distinguished, with the~~ The waves in the 50 m simulation ~~being slightly smaller~~ are now slightly smaller than in the 33 m resolution case. In the ~~two higher 50 and 33~~ m resolution simulations the thermocline has been raised above its rest height behind the leading wave. ~~This is as~~ indicated by the negative surface currents. This feature is missing ~~in the 100 resolution simulation for which the surface currents remain positive between the two leading solitary waves and immediately behind the second solitary wave~~ at lower resolutions. At later times the 50 and 33 m resolution simulations diverge as well, becoming quite different at 85 m depth (Fig. 10d). The back of the leading depression becomes very steep. It is steeper in the 33 m resolution case and is resolved by 4–5 grid ~~points in the 50~~ at both these resolutions. In the 16 m simulation. The jump is steeper in the 33 resolution case the jump is better resolved (7–8 grid points). Wave breaking has commenced behind the two leading depressions just before this time. The steep rear of the waves of depression and the commencement of overturning behind them is similar to that shown in Fig. 5 for bathymetry  $h_0$ . The 16 m resolution case shows much finer details and some weak overturns along the steep rear of the first square-wave depression. At this stage in the evolution of the shoaling waves it is unlikely that the 16 m resolution case has converged. At depths greater than about 140 m the differences between the 50, 33 and 16 m resolution cases are not very significant.

Also shown in Fig. 9d are results [Results](#) from a simulation with  $\Delta x = 33$  m and double the vertical resolution ( $J = 400$ ). ~~These are indistinguishable from the case with half the vertical resolution. See also [are indistinguishable at the scale of Fig. 11 below 10d](#).~~

Similar tests were done using a larger wave (amplitude 115 m) using bathymetry  $h_0$ . This wave is approximately half the width of the 45 m wave, requiring higher horizontal resolutions. The divergence between results for different resolutions was qualitatively similar to that in the above case however the divergence occurred more rapidly. Indeed, after travelling 8.5 km to a depth of 2800 there were already noticeable differences in wave amplitudes between the runs using  $\Delta x = 250, 100$  and 33 m, with the wave in the 250 m resolution simulation already being over 5% smaller than that in the 33 m simulation, suggesting that at a depth of 3000 m the resolution needs to be significantly better than 250 m to accurately simulate waves of this amplitude.

While doubling the vertical resolution did not result in any significant changes in the leading waves it did reduce noise that developed in the deep water behind the waves. When a resolution of 200 grid points was used weak ( $< 0.01 \text{ m s}^{-1}$ ) near surface currents (across the pycnocline at a depth of 50 m) developed over the steepest parts of the bathymetry, indicative of the pressure-gradient error that is intrinsic to sigma-coordinate models. With 400 grid points these currents were reduced by 50%. Simulations with a resolution of 300 and 400 vertical grid points were similar and were very expensive. Because the leading waves were unaffected by increasing the vertical resolution from 200 to 400 we have for the most part used a vertically varying grid with 200 grid points in the vertical. The grid has almost uniformly spaced grid cells for depths greater than 700 m and less than 300 m in deep and shallow water with a transition region centred at 500 m depth. In deep water the resolution was between 21.1 and 21.4 m at depths greater than 700 m and decreases from 6 m in depths at 350 m depth to 5.35 m at the surface. The vertically varying grid better resolves the thermocline in deep water [and improves energy conservation by reducing thickening of the pycnocline by numerical diffusion](#). In water with depths less than 350 m the resolution is almost uniform, with  $dz = 0.4$  m on the shelf. This grid gave virtually identical results to the vertically uniform grid using 400 vertical grid points.

## 3.2 Adiabaticity of shoaling waves

Solitary waves are said to shoal adiabatically if they retain the form of a single solitary wave as they shoal, i.e. no fissioning or reflection occurs (Grimshaw et al., 2004; Vlasenko et al., 2005). This can only occur if the water depth changes sufficiently slowly so that the shoaling wave can adapt to its new depth without shedding significant energy. Adiabatically shoaling waves conserve energy to leading-order in amplitude (in the absence of rotational effects) however they are in general trailed by a long, small amplitude shelf which extends from the back of the solitary wave to the point reached by a wave travelling at the long wave propagation speed generated at the point when the shoaling solitary wave first encounters a depth change (Grimshaw et al., 2004). Because energy is second-order in amplitude the energy in the trailing shelf is negligible, however the mass in the shelf, being first-order in amplitude, can be significant.

In this section we investigate the adiabaticity of the shoaling waves by comparing the leading wave to ISW solutions of the DJL equation having the same total energy as the initial deep water wave. Both bathymetries  $h_0$  and  $h_{15}$  are used. In addition we compare the shoaling behaviour of waves starting in different water depths using bathymetry  $h_0$ . For these comparisons the bathymetries differ only in that they level off at three different deep water depths, namely 3000, 1500 and 1000 m as illustrated in Fig. ~~??~~2b. The base stratification was used except where noted.

Internal wave solutions of the DJL ~~solution equation~~ were computed over a range of water depths for 11 values of the APE:  $25 \text{ MJ m}^{-1}$  and  $50$  to  $500 \text{ MJ m}^{-1}$  in increments of  $50 \text{ MJ m}^{-1}$ . Figure 10a shows the total wave energy  $E$  (KE plus APE) as a function of depth for these 11 values. In Fig. ~~12b~~10b the ratio of kinetic to available potential energy is shown. This ratio is always greater than one for solitary waves (Lamb and Nguyen, 2009). ~~In the deep water (depth~~ At 3000 m ~~) depth~~ this ratio varies from slightly more than 1 to a maximum of 1.2 for the largest wave (amplitude 137 m) for which values are plotted. For larger waves (not shown) this ratio continues to increase, reaching 1.3 for an APE of  $800 \text{ MJ m}^{-1}$  and 1.4 for an APE of  $2 \text{ GJ m}^{-1}$ . The  $800 \text{ MJ m}^{-1}$  wave has an amplitude

of 170 m and a minimum Richardson number of just below 0.25 in the thermocline. The  $2 \text{ GJ m}^{-1}$  wave has an amplitude of 322 m, a minimum Richardson number of 0.11 and the ratio of the maximum current to the propagation speed is  $\max(u)/c = 0.98$ . Waves with  $\max(u)/c > 1$  have cores of recirculating fluid.

As the water depth decreases from 3000 m with the APE fixed the total wave energy increases due to the increasing KE/APE ratio, reaching a peak value at depths between about 400 and 1200 m for small and large waves ( $\text{KE/APE} \approx 1.16$  and 1.3 respectively, see Fig. 10b). As the depth decreases further the total energy rapidly decreases to twice the APE. This near equipartition of energy suggests waves of smaller amplitude. This is indeed borne out in Fig. 11 which shows the wave amplitude (maximum isopycnal displacement), maximum surface current and maximum bottom current (negative for rightward propagating waves of depression) as a function of depth for constant total energies  $E$  of  $50 \text{ MJ m}^{-1}$  and 100 to  $1000 \text{ MJ m}^{-1}$  in increments of  $100 \text{ MJ m}^{-1}$ . These values were obtained by interpolating results from the DJL solutions, for which the APE is prescribed, and will be referred to as the adiabatic curves: these are the curves a shoaling wave would follow if the wave preserved its total energy and had maintained the form of a solitary wave at each for its depth. As the water depth decreases from 3000 m the wave amplitude increases significantly, reaching a maximum value in depths between 300 and 600 m. The largest wave (total energy of  $1 \text{ GJ m}^{-1}$ ) increases in amplitude by a factor of 1.4 from 129 to 183 m. For smaller waves the amplitudes increase by larger factors as the depth decreases (e.g. 3.5, 2.9 and 2.3 for the three smallest waves). Once shallow water is reached the amplitudes decrease rapidly and all waves have an amplitude close to 60 m in water of 200 m depth. This is an indication of the conjugate flow limit being attained: the waves all have the same maximum amplitude and as the wave energy increases the waves get longer with negligible increases in amplitude.

The adiabatic curves are similar for the other two stratifications. Table 3 gives the initial and maximum amplitudes and the depth at which the maximum amplitude occurs for ISW solutions of the DJL equation for waves of fixed total energy. The maximum amplitudes and depths are based on values computed at depth intervals of 50 m. Values for all three strat-

ifications are provided. The increase in amplitude of the waves is similar for stratifications  $\bar{\rho}_b$  and  $\bar{\rho}_1$  while waves using stratification  $\bar{\rho}_2$  show a larger amplitude increase, particularly for small waves.

A similar pattern is seen for the maximum surface currents except that the maximum currents occur in greater depths than do the maximum wave amplitudes and the range of depths at which near-maximum currents occur is much wider than those for near-maximum amplitudes. The bottom currents reach their maximum values in much shallower water and the increase over their deep water values is much larger than the increases in wave amplitude and surface currents.

Figure 11 also shows the maximum wave amplitude, maximum surface current and minimum currents at the bottom from several simulations. ~~Results using bathymetry  $h_0$  (including the modified bathymetries leveling off at depths of 1500 and 1000) are shown in blue while results using bathymetry  $h_{15}$  are shown in red.~~ For these simulations the Coriolis parameter was set to zero, as the adiabatic curves are only appropriate in the absence of rotation. Five simulations were done using bathymetry  $h_0$  ~~for waves starting in a depth of 3000.~~ Four of these used a horizontal resolution of about 33 m with 200 uniformly spaced grid points in the vertical (blue curves). These waves had APEs of 50, 100, 250 and 400  $\text{MJ m}^{-1}$  ~~and are shown with solid blue curves.~~ The fifth case (green dots black dash-dot), also with an APE of 400  $\text{MJ m}^{-1}$ , used double the vertical resolution. It largely overlies the corresponding lower resolution case, ~~although it has slightly larger amplitudes in depths between 600 and 800.~~ Results from ~~four simulations starting at 3000 depth~~ simulations using bathymetry  $h_{15}$  are also shown (red curves). The initial APEs for ~~these waves waves launched from 3000 m depth~~ were 100, 150, 250 and 400  $\text{MJ m}^{-1}$ . ~~Results from simulations starting in shallower depths include one starting~~ The wave started at a depth of 1500 m : ~~The initial wave has an had an initial~~ APE of 375  $\text{MJ m}^{-1}$ , chosen so the total wave energy is similar to that of the wave with an APE of 400  $\text{MJ m}^{-1}$  started at 3000 m depth. ~~Simulations starting at depths of~~ Waves launched from 1000 m ~~used waves with depth had~~ APEs of 50, 60, 70 and 100  $\text{MJ m}^{-1}$ .

Figure 11a and b ~~shown~~ show that the wave amplitudes and maximum surface currents tend to increase more slowly than the adiabatic curves in deep water and follow them more closely in shallow water. The depths at which they begin to follow the adiabatic curves more closely depends on the bathymetry and wave amplitude.

Consider the results obtained using bathymetry  $h_0$  (blue curves) which has a bump at a depth of about 2000 m. When the wave launched at a depth of 3000 m with an APE of  $400 \text{ MJ m}^{-1}$  (initial amplitude 115 m,  $E = 847 \text{ MJ m}^{-1}$ ) first reaches the crest of the bump (depth 1900 m) its amplitude is equal to that of a solitary wave with  $E$  equal to  $750 \text{ MJ m}^{-1}$  while the maximum surface current corresponds to that for a wave with a total energy of  $670 \text{ MJ m}^{-1}$ . By the time the wave has passed over the bump and shoaled to a depth of 1900 m for the second time the wave amplitude and, to a much greater degree, the maximum surface current, have increased to the values corresponding to an ISW with energies closer to that of the original wave. The increase in the maximum surface current is particularly striking. This is an indication the wave is not shoaling adiabatically, i.e. that is it has not fully adjusted to the change in water depth. Results for this wave track an adiabatic curve for depths less than about 1600 m.

~~The wave launched from a depth of 1500 had an APE of 375 chosen so that the total energy (856) was close to that of the first wave. The differences in the wave amplitude and surface current between this wave and the first wave when it arrived at a depth of 1500 (Fig. 11) further illustrate the degree of non-adiabaticity of the shoaling process.~~

Results for the other wave amplitudes are similar. In contrast to the adiabatic curves, the two smallest waves launched from a depth of 3000 m show little increase in the wave amplitude and maximum surface current until they have reached depths of about 750 m, where the bottom slope decreases from 0.03 to 0.004. At this point the amplitude and maximum surface current of the wave with an initial APE of  $100 \text{ MJ m}^{-1}$  ( $E = 204 \text{ MJ m}^{-1}$ ) is well below those for the DJL waves with an initial APE of  $50 \text{ MJ m}^{-1}$ . After this the amplitudes and surface currents rise rapidly and fall tracking the adiabatic curves in depths less than about 700 m. This suggests significantly non-adiabatic shoaling over the steep slope and nearly adiabatic shoaling over the gentle slope between depths of 750 and 80 m. Similar



behaviour is observed for the waves launched from a depth of 1000 m. ~~Of these waves, in depths less than about 700 the wave with an initial APE of 60 has nearly identical amplitude and maximum surface currents to that of the wave with an initial APE of 100 launched from a depth of 3000.~~

Results obtained using bathymetry  $h_{15}$  show a similar pattern. Because this bathymetry is much steeper ~~that~~ than  $h_0$  for depths between 500 and 2300 m, the results with this bathymetry (red curves) do not follow the adiabatic curves until the waves reach much shallower depths of between 500 and 600 m. The effects of the bump at a depth of 600 m are clearly visible. The large loops in the wave amplitudes, particularly evident in the smaller waves, are a consequence of the largest vertically displacements occurring behind the bump after the solitary wave passes over it, rather than in the solitary wave itself, for a short period of time.

In water shallower than about 400 m the large shoaling waves have amplitudes that exceed the conjugate flow limit by as much as 50%: at 350 and 200 m depths the largest shoaling waves have amplitudes of 142 and 95 m while the corresponding conjugate flow amplitudes are 137 and 61 m. Surface currents do not exceed the conjugate flow limits until depths of 250 m are reached. ~~This increase in surface currents is associated with the very steep backs of the waves which are close to overturning for large waves (e.g. see Fig. 14f below).~~

Figure 11c shows the evolution of the ~~largest amplitude~~ strongest bottom currents. The most striking feature ~~of these results~~ is that the bottom currents greatly exceed those for the DJL solutions in water shallower than about 300 m for the large waves and about 200 m for the smaller waves. This is a consequence of the fluid below the thermocline being squeezed out from beneath the waves as the waves shoal which, in shallow water, results in enhanced bottom currents. This has important implications for the occurrence of instabilities, mixing and sediment resuspension beneath the shoaling wave. Also noteworthy is that for the large waves the bottom current increases relative to the adiabatic curves as the waves shoal to about 500 m depth. For the smaller waves they decrease as do the amplitudes and surface

currents. For large waves in shallow water the bottom currents greatly exceed the surface currents.

In summary, the amplitudes and maximum surface and bottom currents of the shoaling waves qualitatively follow the behaviour expected of a wave that is shoaling adiabatically however there are some significant differences, a consequence of the timescale of depth changes experienced by the shoaling wave being shorter than the time required for the waves to adjust to their new depth. The amplitude and surface currents increase more slowly in deep water, particularly over the steep slope between depths of 2250 and 750 m for bathymetry  $h_{15}$ . Part of the difference can be ascribed to the waves having not fully adjusted to the changing depth rather than to fissioning as illustrated by the behaviour as the waves pass over the bump at a depth of 2000 m for bathymetry  $h_0$ . For depths between about 1000 and 400 m the properties of the shoaling waves track the adiabatic curves very well. In shallower water the waves can have amplitudes more than 50% larger than any exact solitary wave at that depth while currents at the bottom can be twice as large.

### 3.3 Sensitivity to initial water depth

Figure ?? For reasons of numerical efficiency it is tempting to truncate the bathymetry and start waves from depths of, say, 1000 m. Here we briefly explore the implications of doing so.

Figure 12 compares the horizontal ~~currents at the surface for the surface current and~~  $\sigma_t = 0.0232 \text{ kgm}^{-3}$  isopycnal at different times for shoaling waves with initial APEs of 60 and  $100 \text{ MJ m}^{-1}$  launched from depths of 1000 and 3000 m respectively using bathymetry  $h_0$ . The latter case is ~~the same one~~ Case 2 illustrated in Fig. 4. ~~Figure ?? shows the corresponding~~  $\sigma_t = 0.0232$  isopycnal at the same times. ~~This isopycnal was chosen because it~~ The chosen isopycnal is at the depth of maximum buoyancy frequency in the undisturbed stratification. It is not the isopycnal which undergoes maximum vertical displacement in the wave. The latter isopycnal varies with wave amplitude and varies as the wave shoals.

These two waves are chosen because in shallow water the leading waves have nearly identical amplitude. At a depth of 750 m ~~the wave launched from a depth of 1000 is about~~ (Fig. 12a,b), ~~where the shelf slope decreases from 0.03 to 0.004, the waves are about~~ 15 km ~~past the bottom of its shelf slope while the wave started from deeper water is about and~~ 150 km beyond the bottom of ~~its shelf slope~~ their shelf slopes. Both waves are asymmetric, with the wave launched from deeper water being much more asymmetric. ~~Recall that at a depth of 750 the shelf slope decreases from 0.03 to 0.004.~~ By the time the wave ~~have~~ has reached a depth of 560 m (Fig. ??b) ~~the initial wave has fissioned into multiple waves. The wave~~ the wave launched from the deeper/shallower water has fissioned into three solitary waves at  $x = -40, -45$  and  $-49$  (the third is just starting to emerge) while the wave launched from the shallower depth has fissioned into two (at  $x = -40$  and  $-46$ ). The leading waves are very similar in amplitude (by choice). ~~By the time the leading waves have reached~~ two solitary waves (not shown). At a depth of 250 m (Fig. ??e 12c,d) the multiple solitary waves produced via fissioning are well separated. ~~In the case of the wave launched in deep water the second wave trails the first by about 9 and the third wave is a further 6 behind.~~ The third wave in Case 2 has a similar amplitude and location to that of the second wave for the case started at 1000 m depth. The pedestal behind the leading wave is starting to form. By the time the waves have reached depths of about 120 m (Fig. ??d) ~~the leading wave has deformed considerably. The wave has broadened considerably. Steep front and backs (at about  $x = 69$  and  $66$ ) are separated by a region in which  $u$  varies slowly and the isopycnals (see Fig. 4d) are close to parallel with the bottom. Behind the leading wave  $u$  is now strongly negative with currents almost equal in magnitude to the positive currents in the leading wave of depression. This is indicative of a large wave shelf trailing the leading wave of depression. The trailing waves have advanced relative to the leading wave as they are in deeper water and have larger propagation speeds. The~~ 12e,f) the third wave in the deep water case has now split into two waves.

As the waves pass the critical point and reach their final depth of 80 m (Fig. ??e and f 12g,h) the leading wave continues to broaden and the currents decay in amplitude. The second wave in the deep water case advances into the wave shelf trailing the leading wave

(the region of negative surface current) with the result that the wave forms behind the leading depression are quite different for the two cases.

### 3.4 Effects of bumps

Truncating the deep water depth to 1000 m significantly modifies the fissioning processes resulting in fewer waves, reducing the relative amplitude of the second solitary wave and increasing the distance between the two leading waves.

#### 3.4 Effects of small scale bumps

The deep bump on bathymetry  $h_0$  does not significantly affect the evolution of the shoaling waves. The much shallower bump on bathymetry  $h_{15}$  has a significant impact. Figure 13 compares the wave fields at  $t = 29$  and 34 h for simulations with and without the bump at 700 depth for an initial wave amplitude of 59 m (APE 150 MJ m<sup>-1</sup>, Case 4). For the bathymetry with the bump the leading three waves at  $t = 29$  h are at  $x = 41.0, 35.9$  and  $31.8$  km. With the bump removed the waves are slightly ahead, at  $x = 42.8, 37.3$  and  $33.7$  km which we attribute to the reduction in propagation speed as the wave passes over the bump. ~~The leading three waves are similar in amplitude when compared at times chosen so that these waves are at the same location with the waves in the no-bump case being slightly larger. This is illustrated in Fig. 13b and d which show the two wave fields at slightly different times, chosen so the leading waves are at approximately the same location.~~ bump also results in a reduction in wave amplitude with the leading three waves containing 60% and 71% of the initial wave energy for cases Cases 4 and 4nb.

The most striking difference between the two simulations is the wave field behind the leading three waves. For bathymetry  $h_{15}$  a Case 4 a small amplitude mode-one wave train trails the leading three waves. Following are higher mode waves, e.g. at time  $t = 29$  (Fig. 16a13a), a concave mode-two wave is centred at about  $x = 16$  km and a convex mode-two wave (and higher mode waves) lies between  $x = 0$  and  $6$  km ~~can be seen~~ with higher mode waves further behind and a wave beam sloping up to the right above the bump.

At the later times mode-two waves in both simulations are clearly apparent but ~~are much larger in the simulation with the bump (e.g.  $t x = 18$  and  $30$ )~~ there is a mode-two concave wave ( $x = 30$  km ~~for the case with a bump, and~~) followed by a train of mode-two waves (between  $x = 16$  and  $20$  km) whereas without the bump there is a single convex mode-two wave at  $x = 20$  km ~~in the case with no bump~~. The bump also results in reflected waves containing about 6% of the initial wave energy (less than the 15% reflected for Case 3 discussed in section 3.1). Without the bump energy in the reflected waves is insignificant.

### 3.5 Sensitivity to initial wave amplitude

Figure 14 compares the shoaling behaviour for three initial waves (amplitudes 45, 83 and 115 m) using the base stratification  $\bar{\rho}_b$  and bathymetry  $h_{15}$  (Cases 3, 6, and 7). Times for comparison are chosen so that the leading waves are in approximately the same location. For the smallest initial wave there are two large solitary waves at  $t = 35$  h (Fig. 14b) whereas for the two larger waves there are three. The intermediate wave has a number of ~~smallers~~ smaller solitary waves trailing the leading large waves that are absent in the two cases with smaller and larger initial waves. ~~Another noticeable feature is that for the largest wave, At the early times shown (panels a, c, e) the leading wave is proportionally much larger than the trailing waves (see Fig. 14f) than in the other two cases. contains 36%, 53% and 75% of the initial wave energy showing a striking increase with the initial wave amplitude. The higher mode waves are similar for these three cases (not shown).~~

### 3.6 Effects of rotation

The effects of rotation on the evolution of the internal tide and on ISWs has been considered by many authors ~~(e.g. Helfrich, 2007; Helfrich and Grimshaw, 2008)~~ (e.g. Helfrich, 2007; Helfrich and Grimshaw, 2008). Rotation makes long wave dispersive and as a consequence ISWs radiate long inertia-gravity (Poincaré) waves behind them and gradually decrease in amplitude. In some regions of parameter space the long radiated waves steepen and form new ISW packets

(Helfrich, 2007). This process takes place on the inertial time period which in the South China Sea is about 32 h. ~~In the deep water, waves propagating at 2.5 will travel close to 300 in one inertial period. As waves shoal their propagation speed decreases and hence waves will be affected by rotation over shorter distances. As our shelf slope systems are on the order of 300 in length.~~ This is comparable to the shoaling times in our simulations so it is clear that rotational effects will significantly affect waves launched from the deep water by the time they reach the shelf.

The effects of rotation on the shoaling of ISWs was investigated using bathymetry  $h_{15}$ . ~~For this stratification the waves were started with the initial waves~~ at  $x = -200$  km. Starting the waves further from the shelf would ~~have increased~~ increase the effects of rotation ~~primarily~~ by reducing the amplitude of the wave at the bottom of the shelf slope and by introducing a long inertia-gravity wave behind the leading solitary wave. As a proxy for ~~this the first effect~~ we can simply consider waves with different initial amplitudes.

Figure 15 compares the  $\sigma_t = 0.0232$  ~~isopycnals at two~~  $\text{kg m}^{-3}$  isopycnals at different times for ~~cases using Cases 3(r) and 5(r), which use~~ two different initial wave amplitudes with, for  $f = 0$  and  $f = 5.35 \times 10^{-5} \text{ s}^{-1}$ . ~~Figure 18a and c~~ Figures 15a–c show results for an initial wave amplitude of 45.4 m (~~case Case 3 and 3r~~). At  $t = 23$  h (Fig. ~~18a15a~~) the leading wave in the non-rotational case is at about  $x = 0$  (depth 610), just past the bump at 610 m depth. The isopycnal undergoes a maximum downward displacement of about 46 m. At this location the  $\sigma_t = 0.0232$  isopycnal is not the isopycnal undergoing maximum displacement ~~—~~ (the amplitude of the leading wave is about 53 m). In the rotational case the leading wave trails by almost 2 km and the isopycnal undergoes a maximum downward displacement of 26 m, almost half that in the non-rotating case. At this point the wave has been travelling for about three quarters of an inertial period and has propagated 200 km. It is no surprise then, that in the rotational case the leading wave has been significantly modified. The long small amplitude wave of elevation between  $x = -25$  and  $-12$  km is slightly larger in the rotational case. The currents in the rotational case are much larger than those in the non-rotating case (not shown). After 35 h (Fig. ~~18e15b~~) the leading waves have reached a depth of about 200 m. At this depth the wave amplitude is strongly controlled by the water depth and

the waves in the non-rotating and rotating cases have similar amplitudes, with the wave in the non-rotating case being much wider. In the non-rotating case three ISWs are present. There are only two in the rotating case. [Figure 18b and d](#) [The wave of elevation between  \$x = 30\$  and  \$50\$  km is larger in the rotating case \(surface currents are twice as strong\) and in the rotating case it subsequently steepens and forms a secondary packet of short waves \(between  \$x = 67\$  to  \$70\$  km at  \$t = 45\$  h, Fig. 15c\) which is not present in the non-rotating case. Such wave packets were reported by Grimshaw et al. \(2014\).](#)

[Figure 15d–e](#) show results for larger initial waves (71.6 m, [case5r](#)). [Similar Cases 5 and 5r](#) and similar trends are observed. [At  \$t = 35\$  packet of small amplitude waves can be seen approximately 50](#) [The secondary wave packet does not form in this case because its formation is disrupted by wave breaking behind the leading waves \(between  \$x = 10\$  and  \$20\$ \). These waves are larger in the rotating case which could be a consequence of the presence of the radiated Poincaré wave mode-one solitary waves. Starting the initial wave further away would give more time for the secondary wave packets to form hence potentially making them more prominent.](#)

In-

Fig. 16 [we plot shows](#) the amplitude of the leading wave as a function of  $x$  as the waves shoal. Results for five pairs of simulations (with and without rotation) using different initial wave amplitudes are shown (cases 3–7). In the absence of rotational effects the waves slowly increase in amplitude until the bump ( $x = -20$  km) is reached. At this stage the wave fissions and the amplitudes of the three smallest waves momentarily decrease. All waves then rapidly increase in amplitude. The largest wave reaches its peak amplitude just before the crest of the bump is reached, then maintains its amplitude before starting to decrease in amplitude rapidly at  $x = 40$  km (420 m depth). The other waves reach their maximum amplitude between  $x = 40$  and  $50$  km (depths of 400–300 m) before rapidly decreasing until the shelf is reached at  $x = 80$  km with smaller waves reaching their maximum amplitude in shallower water.

When rotational effects are included the wave amplitude immediately starts to decrease, approximately linearly with  $x$ . After passing over the bump at  $x = -20$  km the effects of

rotation on the leading wave no longer seem to be prominent. ~~For example, consider case with an initial amplitude of 59 (APE=150). By  $x = -20$  its amplitude is close to that of the smaller wave, with the amplitude varying similarly to those in the non-rotating case. As the waves continue to shoal they remain similar in amplitude although the waves in the rotating case do continue to reduce relative to those in the non-rotating cases. In all cases the waves increase significantly in amplitude after reaching depths of about 800. At 200 depth ( $x = 60.7$ ) all waves significantly exceed the 60 conjugate flow amplitude limit except for the smallest wave with rotational effects.~~

### 3.7 Sensitivity to stratification

#### Figure ??

The stratification at the ASIAEX site varied over the course of the field program. Here we consider the sensitivity of the shoaling behaviour to various in stratification over the course of the program. The major difference in our stratifications is the depth of the thermocline which also acts as a proxy for the raising and lowering of the thermocline in response to the internal tides in the region which are not included in our simulations. Ramp et al. (2004) report on the influence of the internal tides on the wave forms in shallow water.

Figure 17 compares waves fields for ~~two case~~ the three stratifications ( $\bar{\rho}_b$ ,  $\bar{\rho}_1$ , and  $\bar{\rho}_2$ , see Fig. 3) using bathymetry  $h_{15}$ ,  $f = 0$  and an initial wave APE of ~~50~~100 MJ m<sup>-1</sup>. ~~Figure ??a, c, e and b, d, f shows results using density profiles  $\bar{\rho}_1$ . These plots show the leading waves after they have reached the shelf along with trailing mode-one and higher mode waves. For stratification  $\bar{\rho}_b$  (Fig. 17a) the shoaling solitary waves encounter a critical point and  $\bar{\rho}_2$  respectively. Consider stratification  $\bar{\rho}_1$ . Figure 20a shows the leading waves at  $t = 36$  at which point there are two solitary-like waves at  $x = 63$  and 65. They are deforming due to the presence of the bottom showing the typical profile of a steep rear and more gently sloping front. Trailing is a long small amplitude mode-one wave of elevation centred at about  $x = 47$ . This long mode-one wave, being in deeper water, is propagating faster than the leading wave packet and eventually catches up to it (not shown) with little effect because of~~



its small amplitude. Trailing the mode-one waves are mode-two waves. The leading large mode-two wave can be seen at  $x = 47$ – $53$  at  $t = 47$ . Solitary waves are waves of elevation on the shelf. In this case the leading depression is very broad and decays with time. The pedestals will ultimately yield solitary waves of elevation. For stratification  $\bar{\rho}_1$  (Fig. ??e). The mode-two wave is steepening and by  $t = 55$  has evolved into a packet of four mode-two waves with the leading front at  $x = 67$  (17b) the pycnocline is lower in the water column and the critical point is reached at greater depth. In this case breaking has resulted in almost complete destruction of the pedestals. For stratification  $\bar{\rho}_2$  (Fig. ??e). The wave crests are separated by about  $750$  (17b) the pycnocline is above the mid-depth on the shelf and solitary waves of depression persist. In this case it can be seen that the leading depression has a steep front (at approximately  $x = 86$ ). Trailing the packet of short mode-two waves is a long mode-two concave wave ( $x \approx 58$  km) and a long convex mode-two wave ( $x \approx 45$ ). Both convex and concave mode-two internal waves have been observed on the Chinese continental slope in the South China Sea (Yang et al., 2010).

Figure ??b, d and f shows results from a similar case using stratification  $\bar{\rho}_2$ . Figure 20b shows the wave field at  $t = 38$ , in contrast to the other cases. Ultimately a broad square-shaped solitary wave of depression will form. Ramp et al. (2004) observed waves of depression at 120°E. This time was chosen so that the leading wave is at the same location as for the case using  $\bar{\rho}_1$ . In this case there are three solitary-like waves. A long mode-one wave is present during times when the internal tide had raised the thermocline above the mid-depth (their Figure 6, 18:00 GMT May 13 to 06:00 GMT May 14).

In Case 3 ( $\bar{\rho}_1$ , Fig. 17a) a packet of short small amplitude mode-one wave centred at  $x = 45$  km is present between about 60 and 80 km trails the leading wave packet. This wave is larger than the corresponding feature seen in Case 12 ( $\bar{\rho}_2$ , Fig. ??a) and by  $t = 47$  it has steepened to form a second mode-one wave packet seen at  $x = 67$  km (17c) there is a short packet of mode-one wave packet seen at  $x = 67$  km in Fig. ??d at which point a that is not present for the other two stratifications. The mode-two wave packet has just entered the region depicted in the figure. A long concave wave also shows some differences. For Case 9 ( $\bar{\rho}_1$ , Fig. 17b) a long convex

mode-two wave is present at  $x = 53$  between  $x = 44$  and  $50$  km. By  $t = 55$  this wave has sharpened and is more visible ( $x = 65$  in Fig. 20f). For the other stratifications mode-two wave trains have been generated along with concave mode-two waves at  $x = 53$  and  $50$  for Cases 3 and 12 respectively.

Rotation modifies the wave fields (Fig. 20f), as is the trailing 18). The leading mode-one waves on the shelf are similar but smaller in amplitude. The mode-two wave packet.

Figure ?? shows a similar comparison but for cases with rotational effects included. The leading wave packet now consists of a single solitary wave which is smaller than the leading wave in the waves are also similar to those in the corresponding non-rotating cases. At  $t = 43$  for the case with  $\bar{\rho}_1$  a The striking differences between the rotating and non-rotating cases are the large mode-one solitary wave packet can be seen wave packets in the rotational cases (at  $x = 67-70, 69-73$  and  $60-64$  km. This feature is not present in the non-rotating case. It has evolved from the in Cases 3r, 9r, 12r respectively) that have been generated by the nonlinear evolution of the inertia-gravity waves that form behind the shoaling solitary wave. This phenomena was reported by Grimshaw et al. (2014). The mode-one wave that can be seen at  $x = 42$  in Fig. 21a. For  $\bar{\rho}_2$  (Fig. 21d) the mode-one wave packet at  $x = 57$  corresponds to the wave packet seen in the non-rotating case (Fig. ??d). The waves have much larger amplitude was also present in Case 12 but is much larger in the rotating case. The mode-two wave seen Fig. 21e and f are similar to those seen in the non-rotating case.

### 3.8 Effects of viscosity and boundary layer separation

Some simulations were done with vertical eddy viscosity/diffusivity. A vertically varying viscosity/diffusivity of the form

$$\nu = \kappa = K f(z) = K \operatorname{sech} \left( \frac{z - h(x)}{h_s} \right) \quad (3)$$

was used with using a scale height  $h_s = 10.0$  m. The dimensionless function  $f(z)$  is shown in the left panel in Fig. ??19. The diffusivity/viscosity has a maximum value of  $K$  at the

bottom and decreases by factors of 10 and 100 approximately 30 and 53 m above the bottom. This form of the viscosity/diffusivity coupled with a no-slip bottom boundary condition results in flow separation and vortex shedding at the back of the shoaling ISWs (Lamb and Nguyen, 2009; Boegman and Ivey, 2009; Lamb, 2014).

Figure 19 compares results from an inviscid simulation (Fig. 23a and 19a,b) with results from simulations with  $K = 10^{-5}$ ,  $10^{-4}$  and  $10^{-3} \text{ m}^2 \text{ s}^{-1}$ . At the stage illustrated, the four solutions have just become noticeably different in form (when the lead waves are at  $x = 59 \text{ km}$  all four results are very similar with amplitudes decreasing with  $K$ ). For  $K = 10^{-5} \text{ m}^2 \text{ s}^{-1}$  (Fig. 19c,d) the most noticeable difference is the enhancement of the positive near bottom currents behind the leading wave of depression beneath the first pedestal ( $x = 68.5 \text{ km}$ ). This is consistent with flow separation and the formation of a vortex behind the leading depression as has been observed in the laboratory and in lab-scale numerical simulations. This positive current behind the leading depression is strengthened as  $K$  increases. For  $K = 10^{-4} \text{ m}^2 \text{ s}^{-1}$  (Fig. 19e,f) the waves are starting to deform. For the largest value of  $K$  the leading depression is significantly reduced in length and the trailing waves are smaller and show small scale features. In shallower water the differences between the four cases grow.

These results and results from other simulations not shown suggest that viscous effects are not significant until the waves reach depths less than about 200 m however in deeper water the vertical resolution is reduced so these results are merely suggestive. In deep water the near bottom currents are much weaker which would reduce the affects of the bottom boundary layer beneath the shoaling waves. They also show that Observations of sand dunes in the northern South China Sea reported by Reeder et al. (2011) at depths between 160 and 600, m suggest that bottom boundary layer processes could be important at depths greater than 200 m. Our simulations suggest that the presence of a turbulent bottom boundary layer beneath the waves could significantly affect shoaling solitary waves in water depths less than 200 m however these results are quite sensitive to the eddy viscosity. A more detailed investigation is needed.

## 4 Discussion and conclusions

Using a two-dimensional non-hydrostatic primitive equation model we have investigated aspects of the shoaling behaviour of internal solitary waves in the ~~western~~northeastern South China Sea using bathymetry and stratifications based on observations made in the vicinity of the Asian Seas International Acoustic Experiment site (Orr and Mignerey, 2003; Duda et al., 2004; Ramp et al., 2004). Sensitivity to the stratification, the bathymetry and the effects of rotation were considered. The majority of the simulations were done without explicit viscosity. A few runs were done to explore the potential implications of a no-slip bottom boundary condition and the presence of a turbulent bottom boundary layer. Consideration of the effects of concurrent barotropic tides on shoaling ISWs are left for future work.

While waves with amplitudes close to 200 m have been observed in the deep part of the South China Sea (Klymak et al., 2006; Lien et al., 2012, 2014), we considered initial waves with amplitudes between 30 and 115 m in water 3000 m deep which are more typical (Li and Farmer, 2011). The adiabaticity of the shoaling was considered by tracking the wave amplitude and maximum wave induced currents as a function of water depth as the waves shoaled and comparing them with values ~~for~~along the adiabatic curves (internal solitary waves with ~~the same energy~~constant energy). We found some significant deviations from the adiabatic curves, with the amplitudes and currents during shoaling being significant less than those for an adiabatically shoaling wave. Thus the bathymetry in the vicinity of the ASIAEX site is steep enough to result in significant deviations of the shoaling wave from a solitary wave solution of the DJL equation with the same initial energy. Some energy is lost by fissioning of the initial wave into multiple waves. An example is that of Case 2 shown in Figs. 4 and 5. This case also illustrates the common occurrence of wave breaking in waves behind the leading depression (in this case at the back of the third wave of depression). Because of the very steep rear of the shoaling waves high horizontal resolutions were necessary. For most of our simulations we used a horizontal resolution of 33 m. The trailing waves did depend on the initial water depths. Comparisons of the shoaling behaviour of solitary waves with different deep water depths were done in which we tuned the amplitude

of the wave starting in water of 1000 and 1500 m depths so that in water depths of less than 1000 m the leading waves had the same amplitude. The wave starting in the deeper water had larger trailing waves, an indication of the non-adiabatic nature of the shoaling even in deep water. Thus, in order to make detailed comparisons with observations it will be important to start at an appropriate deep water depth.

The bumps on the shelf slope topography influenced the shoaling behaviour, particularly the shallower bump on bathymetry  $h_{15}$  which is about 200 m high in water 700 m deep. As the shoaling wave passes over this bump higher mode waves are formed. As the bumps in the bathymetric transects are slices through three-dimensional features this implies that three-dimensionality of the bathymetry is likely an important factor in some locations, particularly for the secondary waves that form during shoaling.

In the absence of rotation, shoaling waves grow slightly in amplitude until they reach water depths of 800–1000 m after which they rapidly grow, reaching their maximum amplitude at depths between 250 and 600 m for initial amplitudes of 45 and 115 m respectively. They then decrease rapidly in amplitude but large waves can be 50 % larger than the conjugate flow amplitude limit in water of 200 m depth. Rotation results in a continuous decrease in wave amplitude as waves shoal from 3000 m depth to 1000 m depth due to the continual radiation of inertia-gravity waves, but thereafter the waves undergo the same rapid rise and fall of their amplitude as ~~the~~they shoal into shallower water.

Ramp et al. (2004) presented time-depth temperature contour plots of internal waves at depths of 350, 200 and 120 m spanning an 11 day period. At 350 m depth they reported wave amplitudes (based on the 24° isotherm, hence amplitudes potentially underestimated) ranging between 29 and 142 m which matches well with the range of amplitudes in our simulations. Many features of the observed waves are similar to those seen in our simulations although there is naturally a great deal of variability in the observed waves. At 350 m depth ~~waves~~ both the observed and simulated waves were fairly symmetric. At 200 m depth many of the observed waves and all of the simulated waves were quite asymmetric (see also Fig. 4 in Orr and Mignerey, 2003 which shows acoustic images of an asymmetric wave close to this depth). As an example of a wave which is similar to one of our simulations

consider the  $a$  wave observed at 08:00 GMT on 7 May (see Fig. 4 and Table III in Ramp et al., 2004). At 350 m depth it had an amplitude of 110 m and appears reasonably symmetric (note, however the difference in stratifications ahead and behind the wave suggesting that the observed wave is propagating at the front of a long depression). Four hours later it arrived at the 200 m depth mooring at which point it is quite asymmetric with the back of the wave being much steeper than the front of the wave. In our Case 6, which had an initial amplitude of 83.1 m, the leading wave had an amplitude of 117 m at 350 m depth at which point it was about 1.5 km in width and had a propagation speed of  $1.6 \text{ m s}^{-1}$ . Ramp et al. (2004) report a propagation speed of  $1.33 \text{ m s}^{-1}$  and a width of 760 m (twice their reported half-width) for their observed wave. At 200 m depth the wave in our simulation had widened to 2 km and the propagation speed had decreased to  $1.0 \text{ m s}^{-1}$ . The wave was also asymmetric as is the observed wave (Ramp et al., 2004). Using a propagation speed of  $1 \text{ m s}^{-1}$  the observed wave also has a width of about 2 km. By the time the observed waves have reached a depth of 120 m they have broken up into many smaller waves including waves of elevation superimposed on broad depressions. Our simulations with viscosity suggest that by this depth the waves may have been strongly modified by bottom boundary layer processes.

Many of the observations from the ASIAEX program show waves that are broad, with a gently sloping front and steep back, in water of 120 and 85 m depth (Ramp et al., 2004; Lynch et al., 2004; Duda et al., 2004). These are often trailed by a small number of narrow waves of elevation and square shaped depressions as in our simulations. Figure 3 in Duda et al. (2004) shows the presence of waves of elevation in which the thermocline is raised above its rest height in a water depth of 85 m similar to the pedestals generated in our simulations. Ramp et al. (2004) show several examples (e.g., 14:00-16:00 GMT on May 7, 15:00-16:00 GMT on May 9, their Figure 6) in which near bottom water is raised well into the water column in waves of elevation trailing a broad wave of depression in water of 120 m depth.

In our simulations we start with a single solitary wave in deep water. The shoaling wave fissions into several waves, with at least two well separated solitary waves having

been formed by depths of 600–700 m for both bathymetries, with the waves separating at greater depth for bathymetry  $h_0$  which has the more gentle slope. For the steeper bathymetry the waves have reached shallower water before completely separating. In contrast, Lynch et al. (2004) and Ramp et al. (2004) report that large solitary waves at a depth of 350 m have split into two by the time they reach a depth of 200 m.

During the ASIAEX program only one mode-two wave was observed (Lynch et al., 2004). Yang et al. (2004, 2009, 2010) analyzed mooring data in the vicinity of the ASIAEX field program. The moorings were deployed on the continental shelf at several locations by various experiments with their analysis focusing on the upper 400 m of the water column. Time series measurements of temperature and currents indicated the presence of mode-1 and mode-2 ISWs. Many mode-two waves were observed during the VANS/WISE field programs (Yang et al., 2009, 2010). Two types were reported: convex mode-two waves in which there is a bulge in the thermocline with isotherms raised/lowered in the upper/lower part of the water column, and concave mode-two waves with isotherms displaced in the opposite directions. Convex mode-two waves were by far the most common as is the case in our simulations (see below). These structures occurred at the moorings located at various sites on the continental shelf. It was suggested that mode 2 structures were locally generated involving nonlinear effects and topography structure. Stratification and seasonal variations played a role in generation of mode 2 ISWs (Yang et al., 2010).

Our simulations also showed the formation of both convex and concave mode-two waves by which evolved from the shoaling mode-one wave, as observed by Yang et al. (2009, 2010). ~~These were more prominent for bathymetry  $h_{15}$  which had the shallow bump, and their~~ Their presence and amplitude were sensitive to the stratification and to rotational effects. ~~The shallow bump on bathymetry  $h_{15}$  led to the generation of a mode-two wave train and made the mode-two ISWs more prominent (see Fig. 13). The generation mechanisms of mode-two ISWs, their frequency of occurrence, and locations on the continental shelf require further study.~~

An important process not considered in this study is the influence of barotropic tides and background currents on the shoaling of internal solitary waves. The advection of the

shoaling wave by on-shelf and off-shelf tidal currents will decrease and increase the time the waves have to adjust – effectively increasing and decreasing the slope. In addition the on- and off-shelf motion will modify the stratification experienced by the waves and will generate other waves for the shoaling wave to interact with. Our simulations with near-bottom eddy viscosity suggest that the shoaling waves may be significantly modified by viscous effects in water shallower than 200 m, though our simulations are not well resolved in deep water so this remains an open question. Clearly much remains for us to learn about the evolution of shoaling ISWs.

*Acknowledgements.* This work is supported by the Office of Naval Research under PE 62435 (A. Warn-Varnas) and grants from the Natural Sciences and Engineering Research Council of Canada and the Canadian Foundation for Innovation (K. Lamb).

## References

- [Alford, M. H., Lien, R. C., Simmons, H., Klymak, J., Ramp, S., Yang, Y. J., Tang, D., and M.-H. Chang.: Speed and evolution of nonlinear internal waves transiting the South China Sea, \*J. Phys. Oceanogr.\*, \*\*40\*\*, 1338–1355, doi:10.1175/2010JPO4388.1, 2010.](#)
- Apel, J. R., Holbrook, J. R., Liu, A. K., and Tsai, J. J.: The Sulu Sea internal soliton experiment, *J. Phys. Oceanogr.*, **15**, 1625–1641, 1985.
- Boegman, L. and Ivey, G. N.: Flow separation and resuspension beneath shoaling nonlinear internal waves, *J. Geophys. Res.*, **114**, c02018, doi:10.1029/2007JC004411, 2009.
- Buijsman, M. C., Kanarska, Y., and McWilliams, J. C.: On the generation and evolution of nonlinear internal waves in the South China Sea, *J. Geophys. Res.*, **115**, C10057, doi:10.1029/2009JC006004, 2010.
- Duda, T. F., Lynch, J. F., Irish, J. D., Beardsley, R. C., Ramp, S. R., Chiu, C.-S., Tang, T. Y., and Y.-J. Yang: Internal tide and nonlinear wave behavior at the continental slope in the northern South China Sea, *IEEE J. Oceanic Eng.*, **29**, 1105–1130, doi:10.1109/JOE.2004.836998, 2004.
- Farmer, D., Li, Q., and Park, J.-H.: Internal wave observations in the South China Sea: the role of rotation and non-linearity, *Atmos. Ocean.*, **47**, 267–280, doi:10.3137/OC313.2009, 2009.



- Grimshaw, R., Pelinovsky, E., and Poloukhina, O.: Higher-order Korteweg-de Vries models for internal solitary waves in a stratified shear flow with a free surface, *Nonlin. Processes Geophys.*, 9, 221–235, doi:10.5194/npg-9-221-2002, 2002.
- Grimshaw, R., Pelinovsky, E. N., Talipova, T. G., and Kurkin, A.: Simulations of the transformation of internal solitary waves on oceanic shelves, *J. Phys. Oceanogr.*, 34, 2774–2791, 2004.
- [Grimshaw, R., Guo, C., Helfrich, K., and Vlasenko, V.: Combined effect of rotation and topography on shoaling oceanic internal solitary waves, \*J. Phys. Oceanogr.\*, 44, 1116–1132, doi:10.1175/JPO-D-13-1094.1, 2014.](#)
- Guo, C. and Chen, X.: A review of internal solitary wave dynamics in the northern South China Sea, *Prog. Oceanogr.*, 121, 7–23, doi:10.1016/j.pocean.2013.04.002, 2014.
- Helfrich, K. R.: Internal solitary wave breaking and run-up on a Uniform Slope, *J. Fluid Mech.*, 243, 133–154, 1992.
- Helfrich, K. R.: Decay and return of internal solitary waves with rotation, *Phys. Fluids*, 19, 026601, doi:10.1063/1.2472509, 2007.
- Helfrich, K. R. and Grimshaw, R. H. J.: Nonlinear Disintegration of the Internal Tide, *J. Phys. Oceanogr.*, 38, 686–701, doi:10.1175/2007JPO3826.1, 2008.
- Helfrich, K. R. and Melville, W. K.: On long nonlinear internal waves over slope-shelf topography, *J. Fluid Mech.*, 167, 285–308, 1986.
- Hodges, B., Laval, B., and Wadzuk, B.: Numerical error assessment and a temporal horizon for internal waves in a hydrostatic model, *Ocean Model.*, 13, 44–64, doi:10.1016/j.ocemod.2005.09.005, 2006.
- Hsu, M.-K. and Liu, A. K.: Nonlinear internal waves in the South China Sea, *Can. J. Remote Sens.*, 26, 72–81, 2000.
- Klymak, J. M., Pinkel, R., Liu, C.-T., Liu, A. K., and David, L.: Prototypical solitons in the South China Sea, *Geophys. Res. Lett.*, 33, L11607, doi:10.1029/2006GL025932, 2006.
- Lamb, K. G.: Numerical experiments of internal wave generation by strong tidal flow across a finite amplitude bank edge, *J. Geophys. Res.*, 99, 843–864, 1994.
- Lamb, K. G.: A numerical investigation of solitary internal waves with trapped cores formed via shoaling, *J. Fluid Mech.*, 451, 109–144, 2002.
- [Lamb, K. G.: Shoaling solitary internal waves: on a criterion for the formation of waves with trapped cores, \*J. Fluid Mech.\*, 478, 81–100, 2003.](#)
- Lamb, K. G.: Energy and pseudoenergy flux in the internal wave field generated by tidal flow over topography, *Cont. Shelf Res.*, 27, 1208–1232, doi:10.1016/j.csr.2007.01.020, 2007.

- Lamb, K. G.: Internal wave breaking and dissipation mechanisms on the continental slope/shelf, *Ann. Rev. Fluid Mech.*, 46, 231–254, doi:10.1146/annurev-fluid-011212-140701, 2014.
- Lamb, K. G. and Nguyen, V. T.: Calculating energy flux in internal solitary waves with an application to reflectance, *J. Phys. Oceanogr.*, 39, 559–580, doi:10.1175/2008JPO3882.1, 2009.
- Lamb, K. G. and Wan, B.: Conjugate flows and flat solitary waves for a continuously stratified fluid, *Phys. Fluids*, 10, 2061–2079, 1998.
- Lamb, K. G. and Yan, L.: The evolution of internal wave undular bores: comparisons of a fully nonlinear numerical model with weakly nonlinear theory, *J. Phys. Oceanogr.*, 26, 2712–2734, 1996.
- Li, Q. and Farmer, D. M.: The generation and evolution of nonlinear internal waves in the deep basin of the South China Sea, *J. Phys. Oceanogr.*, 41, 1345–1363, doi:10.1175/2011JPO4587.1, 2011.
- Lien, R.-C., D’Asaro, E., Henyey, F., Chang, M. H., Tang, T. Y., and Yang, Y. J.: Trapped core formation within a shoaling nonlinear internal wave, *J. Phys. Oceanogr.*, 42, 511–525, doi:10.1175/2011JPO4578.1, 2012.
- Lien, R.-C., Henyey, F., Ma, B., and Yang, Y. J.: Large-amplitude internal solitary waves observed in the northern South China Sea: properties and energetics, *J. Phys. Oceanogr.*, 44, 1095–1115, doi:10.1175/JPO-D-13-088.1, 2014.
- Liu, A. K., Chang, Y. S., Hsu, M.-K., and Liang, N. K.: Evolution of nonlinear internal waves in the East and South China Seas, *J. Geophys. Res.*, 103, 7995–8008, 1998.
- Lynch, J. F., Ramp, S. R., Chiu, C.-S., Tang, T. Y., Yang, Y.-J., and Simmen, J. A.: Research highlights from the Asian Seas International Acoustics Experiment in the South China Sea, *IEEE J. Oceanic Eng.*, 29, 1067–1074, doi:10.1109/JOE.2005.843162, 2004.
- Niwa, Y. and Hibiya, T.: Numerical study of the spatial distribution of the  $M_2$  internal tide in the Pacific Ocean, *J. Geophys. Res.*, 106, 22441–22449, 2001.
- Niwa, Y. and Hibiya, T.: Three-dimensional numerical simulation of  $M_2$  internal tides in the East China Sea, *J. Geophys. Res.*, 106, C04027, doi:10.1029/2003JC001923, 2004.
- Orr, M. H. and Mignerey, P. C.: Nonlinear internal waves in the South China Sea: observation of the conversion of depression internal waves to elevation internal waves, *J. Geophys. Res.*, 108, 3064, doi:10.1029/2001JC001163, 2003.
- Osborne, A. R. and Burch, T. L.: Internal solitons in the Andaman Sea, *Science*, 208, 451–460, 1980.
- Ramp, S. R., Tang, T. Y., Duda, T. F., Lynch, J. F., Liu, A. K., Chiu, C.-S., Bahr, F. L., Kim, H.-R., and Yang, Y.-J.: Internal solitons in the northeastern South China Sea, Part I: Sources and deep water propagation, *IEEE J. Oceanic Eng.*, 29, 1157–1181, doi:10.1109/JOE.2004.840839, 2004.

- [Reeder, D. B., Ma, B. B., and Yang, Y. J.: Very large subaqueous sand dunes on the upper continental slope in the South China Sea generated by episodic, shoaling deep-water internal solitary waves, \*Mar. Geol.\*, \*\*279\*\*, 12–18, doi:10.1016/j.margeo.2010.10.009, 2011.](#)
- [St. Laurent, L.: Turbulent dissipation on the margins of the South China Sea, \*Geophys. Res. Lett.\*, \*\*35\*\*, L23615, doi:10.1029/2008GL035520, 2008.](#)
- [Stastna, M. and Lamb, K. G.: Large fully nonlinear internal solitary waves: the effect of background current, \*Phys. Fluids\*, \*\*14\*\*, 987–2999, 2002.](#)
- Vitousek, S. and Fringer, O. B.: Physical vs. numerical dispersion in nonhydrostatic ocean modeling, *Ocean Model.*, **40**, 72–86, doi:10.1016/j.ocemod.2011.07.002, 2011.
- Vlasenko, V. and Hutter, K.: Numerical experiments on the breaking of solitary internal waves over a slope-shelf topography, *J. Phys. Oceanogr.*, **32**, 1779–1793, 2002.
- Vlasenko, V. and Stashchuk, N.: Three-dimensional shoaling of large-amplitude internal waves, *J. Geophys. Res.*, **112**, C11018, doi:10.1029/2007JC004107, 2007.
- Vlasenko, V., Ostrovsky, L., and Hutter, K.: Adiabatic behavior of strongly nonlinear internal solitary waves in slope-shelf areas, *J. Geophys. Res.*, **110**, C04006, doi:10.1029/2004JC002705, 2005.
- Vlasenko, V., Guo, C., and Stashchuk, N.: On the Mechanism of A-type and B-type internal solitary wave generation in the northern South China Sea, *Deep-Sea Res. Pt. I*, **69**, 100–112, doi:10.1016/j.dsr.2012.07.004, 2012.
- [Wang, Y.-H., Dai, C.-F., and Chen, Y.-Y.: Physical and ecological processes of internal waves on an isolated reef ecosystem in the South China Sea, \*Geophys. Res. Lett.\*, \*\*34\*\*, L18609, doi:10.1029/2007GL030658, 2007.](#)
- Warn-Varnas, A., Hawkins, J., Lamb, K. G., Piacsek, S., Chin-Bing, S., King, D., and Burgos, G.: Solitary wave generation dynamics at Luzon Strait, *Ocean Model.*, **31**, 9–27, doi:10.1016/j.ocemod.2009.08.002, 2010.
- [Yang, Y. J., Tang, T. Y., Chang, M. H., Lui, A. K., Hsu, M.-K., and Ramp, S. R.: Solitons Northeast of Tung-Sha Island during the ASIAEX pilot studies, \*IEEE J. Oceanic Eng.\*, \*\*29\*\*, 1182–1199, doi:10.1109/JOE.2004.841424, 2004.](#)
- Yang, Y. J., Fang, Y. C., Chang, M.-H., Ramp, S. R., Kao, C.-C., and Tang, T. Y.: Observations of Second Baroclinic Mode Internal Solitary Waves on the Continental Slope of the Northern South China Sea, *J. Geophys. Res.*, **114**, C10003, doi:10.1029/2009JC005318, 2009.
- Yang, Y. J., Fang, Y. C., Tang, T. Y., and Ramp, S. R.: Convex and concave types of second baroclinic mode internal solitary waves, *Nonlin. Processes Geophys.*, **17**, 605–614, doi:10.5194/npg-17-605-2010, 2010.

Zhao, X. and Alford, M. H.: Source and propagation of internal solitary waves in the northeastern South China Sea, J. Geophys. Res., 111, c11012, doi:10.1029/2006JC003644, [1989-2006](#).

**Table 1.** Properties of Initial ISWs in 3000 m depth.  $\bar{\rho}$  is the density stratification used,  $\bar{E}_a$  and  $\bar{E}_k$  are the available potential energy and kinetic energy of the wave,  $a$  is the wave amplitude (maximum isopycnal displacement),  $c$  the wave propagation speed and  $U_{max}$  is the maximum horizontal current in the wave.

$\bar{\rho}$	$\bar{E}_a$ (MJ m <sup>-1</sup> )	$\bar{E}_k$ (MJ m <sup>-1</sup> )	$a$ (m)	$c$ (m s <sup>-1</sup> )	$U_{max}$ (m s <sup>-1</sup> )
$\bar{\rho}_b$	70.0	72.3	35.9	2.53	0.35
–	100.0	104.3	45.4	2.56	0.46
–	150.0	158.6	59.3	2.61	0.62
–	200.0	214.2	71.6	2.64	0.77
–	250.0	271.2	83.1	2.68	0.93
–	300.0	329.7	93.9	2.72	1.11
–	350.0	390.4	104.5	2.76	1.30
–	400.0	454.6	115.2	2.81	1.53
$\bar{\rho}_1$	50.0	51.0	26.29	2.57	0.23
–	100.0	103.2	41.72	2.60	0.38
–	150.0	156.6	54.70	2.64	0.53
$\bar{\rho}_2$	50.0	50.8	26.20	2.51	0.20
–	100.0	102.6	41.43	2.54	0.32
–	150.0	155.3	54.11	2.56	0.43

**Table 2.** Maximum increase in wave amplitude of ISW solutions of the DJL equation. Shoaling cases starting at 3000 m depth. First column is total energy (available potential energy cases run using bathymetry  $h_{15}$  without the bump are indicated with an optional nb and kinetic energy) cases run with rotation turned on are indicated by an optional r.  $a_{3000}$  is the wave amplitude in a water depth of 3000 m. Three sets of simulations were run with and without viscosity.  $\max a$  is the maximum wave amplitude for the given energy,  $d_{\max}$  is the water depth where the maximum occurs ( $\nu$ ). The Cases numbers with an optional  $\nu$  indicate cases run with viscosity. For these cases three values separated by  $\nu$  were used, the value of  $\nu$  being indicated by  $l$  are values for densities  $\bar{\rho}_b$  a number,  $\bar{\rho}_1$  and  $\bar{\rho}_2$ . Values based on  $g$ ,  $\nu n$  where values calculated at depth intervals of 50 m,  $n = 3, 4,$  or  $5$  are for  $K = 10^{-n}$  (see Fig m<sup>2</sup> s<sup>-1</sup>. -11) Thus Case 4nb was run with the bump removed and Case 4\_r was the same as Case 4 but with rotation turned on. Case 9 $\nu$ 4 was run with a viscosity using  $K = 10^{-4}$  m<sup>2</sup> s<sup>-1</sup>.

Case	$\rho$	$\bar{E}_a$ (MJ m <sup>-1</sup> )	$a$ (m)	Bathymetry
1	$\rho_b$	50	28.7	$h_0$
2	—	100	45.4	—
3(r)	—	100	—	$h_{15}$
4(nb)_(r)	—	150	59.3	—
5(r)	—	200	71.6	—
6(r)	—	250	83.1	—
7(r)	—	400	115.3	—
8(r) ( $\nu$ )	$\rho_1$	50	26.3	—
9( $\nu$ )	—	100	41.7	—
10( $\nu$ )	—	150	54.7	—
11(r)	$\rho_2$	50	26.2	—
12	—	100	41.4	—
13	—	150	54.1	—

**Table 3.** Maximum increase in wave amplitude of ISW solutions of the DJL equation. First column is total energy (available potential and kinetic energy),  $a_{3000}$  is the wave amplitude in a water depth of 3000 m,  $\max a$  is the maximum wave amplitude for the given energy,  $d_{\max}$  is the water depth where the maximum occurs. The three values separated by / are values for densities  $\bar{\rho}_b$ ,  $\bar{\rho}_1$  and  $\bar{\rho}_2$ . Given values are based on DJL solutions calculated at depth intervals of 50 m (see Fig. 11).

$\bar{E}$ (MJ m <sup>-1</sup> )	$a_{3000}$ (m)	$\max a$ (m)	$\frac{\max a}{a_{3000}}$	$d_{\max}$ (m)
50	18/16/18	62/56/70	3.4/3.4/4.2	250/300/250
100	28/28/26	81/74/89	2.9/2.8/3.4	300/350/300
200	45/41/41	105/98/113	2.3/2.4/2.7	400/400/350
400	70/65/64	134/127/142	1.9/2.0/2.2	450/500/450
600	91/85/84	154/147/162	1.7/1.7/1.9	500/600/500
1000	129/120/116	183/178/191	1.4/1.4/1.6	600/600/600

Shoaling cases starting at 3000 depth. Cases run using bathymetry  $h_{15}$  without the bump are indicated with an optional nb and cases run with rotation turned on are indicated by an optional r. Three sets of simulations were run with and without viscosity. These are indicated by the ( $\nu$ ). Cases numbers with an optional  $\nu n$  for  $n = 3, 4$ , or  $5$  are for for  $K = 10^{-n}$ . Thus Case 4nb was run with the bump removed and Case 4 was the same as Case 4 but with rotation turned on. Cases run with viscosity are indicated by the ( $\nu$ ). The viscosity cases were run for the three different values of  $\nu$ .

Case  $\rho \bar{E}_a$  ( $a$ ) Bathymetry 1  $\rho_b$  50 28.7  $h_0$  2 – 100 45.4 – 3(r) – 100 –  $h_{15}$  4(nb)(r) – 150 59.3 – 5(r) – 200 71.6 – 6(r) – 250 83.1 – 7(r) – 400 115.3 – 8(r) ( $\nu$ )  $\rho_1$  50 26.3 – 9( $\nu$ ) – 100 41.7 – 10( $\nu$ ) – 150 54.7 – 11(r)  $\rho_2$  50 26.2 – 12 – 100 41.4 – 13 – 100 54.1 –

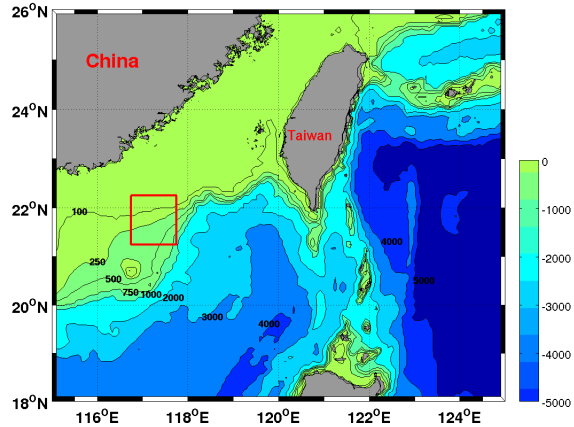


**Figure 1.** Luzon Strait and South China Sea region. Red square is location of ASIAEX experimental site. Colours show depth in meters.



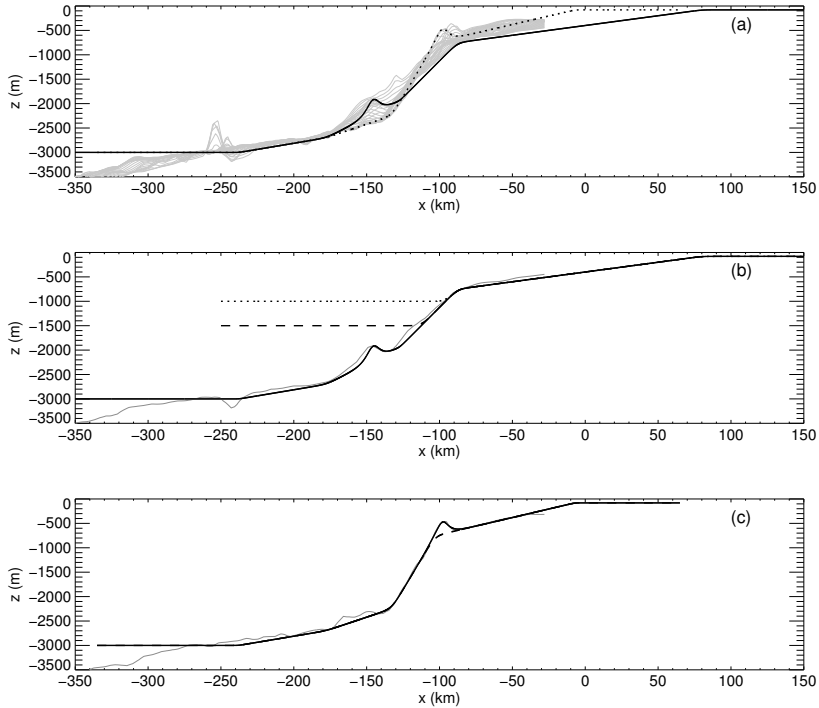


**Figure 2.** Sample measured bathymetries at the ASIAEX location extracted from the Digital Bathymetry 2 min resolution (DB2) data base inside the red square area in Fig. 1. **(a)** Comparison of 24 different measured bathymetries (grey) with two model bathymetry (solid and dotted black curves). **(b)** Comparison of first model bathymetry,  $h_0$ , (black) with one of the measured bathymetries (grey). The bathymetries used for simulations starting at depths of 1000 and 1500 m are also shown. **(c)** Comparison of two other model bathymetries (solid and dashed black curves) with a second measured bathymetry (grey). The solid curve is bathymetry  $h_{15}$ . The dashed curved is the same bathymetry with the bump at  $-100$  km removed.

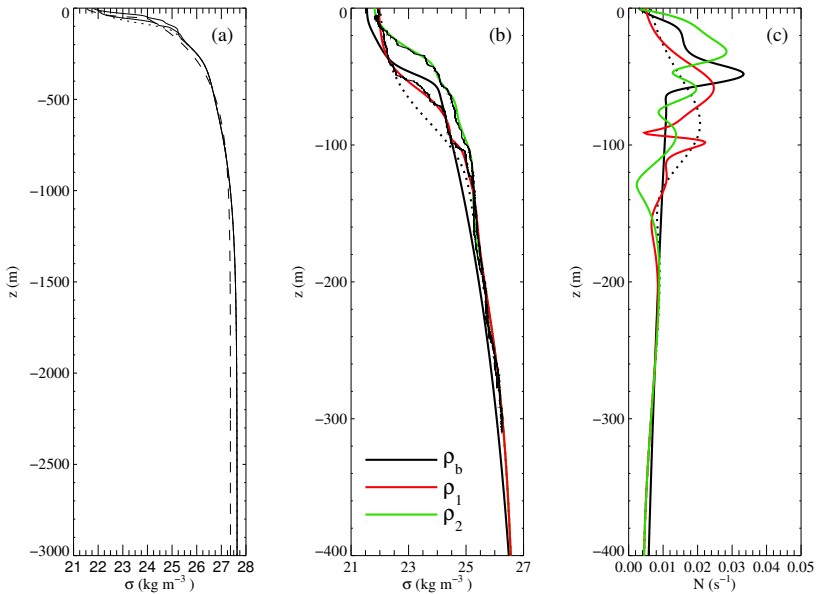


**Figure 3.** Stratifications. **(a, b)**  $\sigma = \rho - 1000 \text{ kg m}^{-3}$  for the base stratification (dashed) and two fits to observed stratifications (solid). Lower solid curve is  $\bar{\rho}_1$ . Upper solid curve is  $\bar{\rho}_2$ . For comparison the dotted line is the Luzon Strait stratification used in Warn-Varnas et al. (2010). **(e)** **(b)** Stratifications in upper 400 m. Base stratification (thick black curve),  $\bar{\rho}_1$  (red),  $\bar{\rho}_2$  (green) and Luzon Strait stratification (dotted). Thin solid lines show corresponding observed density profile. **(d)** **(c)**  $N$  (rad s<sup>-1</sup>) for model stratifications shown in **(e)** **(b)**.

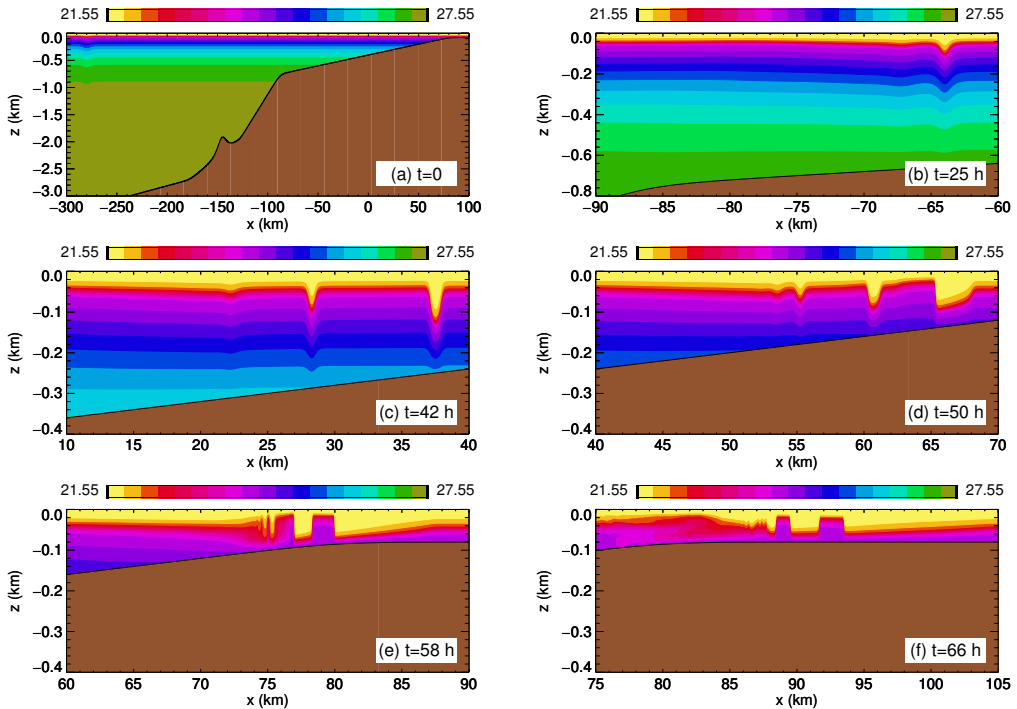


**Figure 4.** Conjugate flow amplitudes as Density fields for Case 2 using bathymetry  $h_0$ . Resolution:  $\Delta x = 33$  m,  $J = 400$ . Initial wave amplitude 45 m. (a) 0 h (full depth shown). (b) 25 h. (c) 42 h. (d) 50 h. (e) 58 h. (f) 66 h. The initial wave at  $x = -280$  km is barely detectable at this scale. Panel (a function of) shows the full depth for stratification  $\bar{\rho}_b$ , panel (b) the upper 800 m and the remainder of the upper 400 m of the water column. Density values are  $\sigma$  in  $\text{kg m}^{-3}$ .

Density fields for Case 2 using bathymetry  $h_0$ . Resolution:  $\Delta x = 33$ ,  $J = 400$ . Initial wave amplitude 45. (a) 0. (b) 25. (c) 42. (d) 50. (e) 58. (f) 66. The initial wave at  $x = -280$  is barely detectable at this scale.

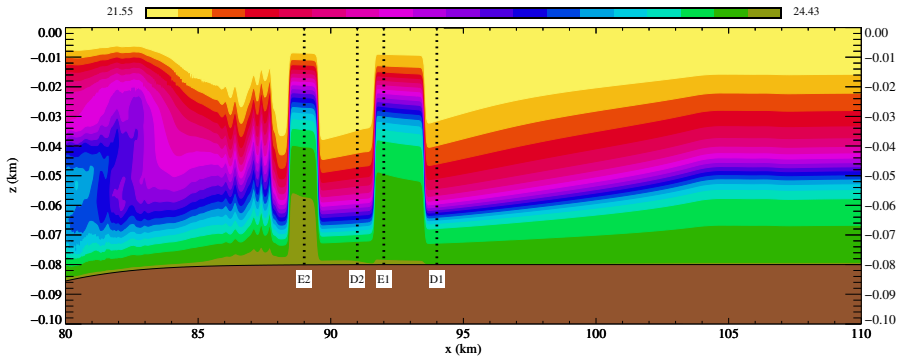


**Figure 5.** Close up of shoaling waves from Case 2 at  $t = 66$  h shown in Fig. 4f showing onset of breaking behind the leading two waves. Vertical dashed lines are locations of vertical profiles shown in Fig. 6.

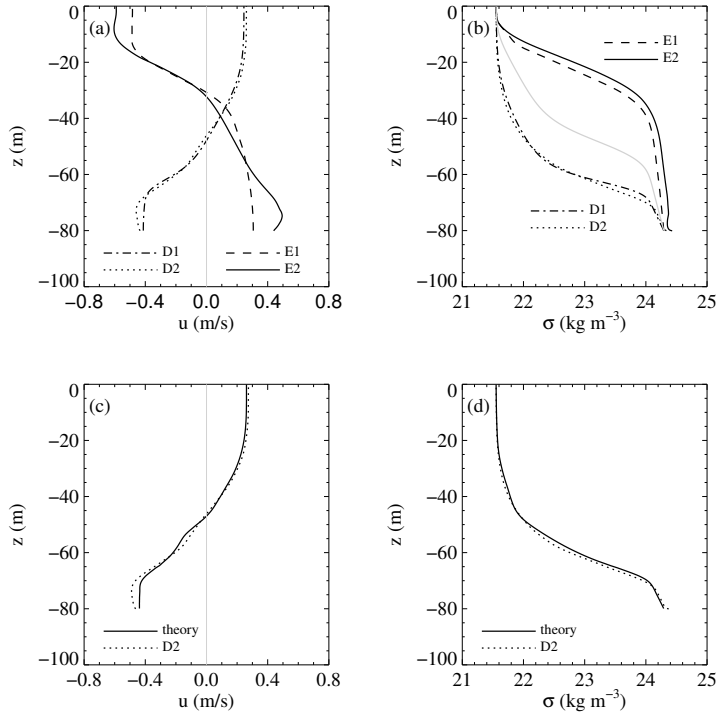


**Figure 6.** (a, b) Vertical profiles of horizontal velocity and density for Case 2 at  $t = 66$  h at locations shown in Fig. 5. (a) Horizontal velocity. (b) Density. Curves from second wave pedestal at  $x = 89$  km (solid), the second depression at  $x = 91$  km (dots), the first pedestal at  $x = 92$  km (dashed), and in the leading depression at  $x = 94$  km (dash-dot) (see Fig. 5 for profile locations). The light grey curve in (b) shows the background density profile. (c, d) Profiles in solitary waves of depression (solid) computed on background field given by profiles extracted from simulation in the pedestal at  $x = 92$  km between the two leading waves of depression. Solution is compared with profiles taken from the second depression at  $x = 91$  km (dots).

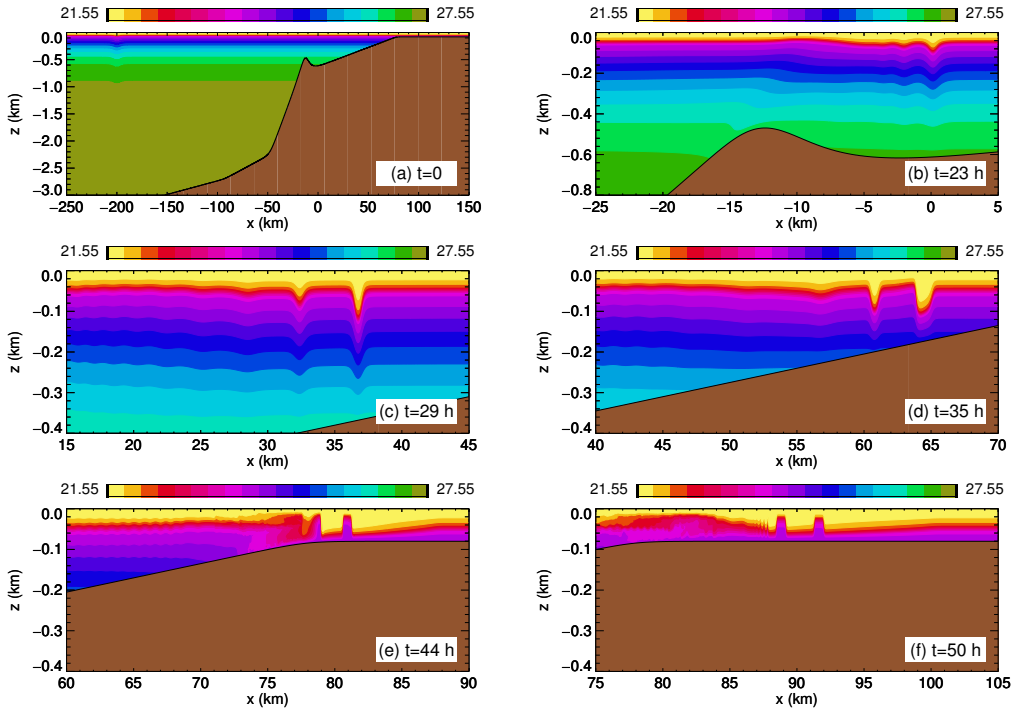


**Figure 7.** Density fields for Case 3 using bathymetry  $h_{15}$  and stratification  $\bar{\rho}_b$ . Resolution:  $\Delta x = 33$  m,  $J = 400$ . Initial wave amplitude 45 m, (APE = 100 MJ m<sup>-1</sup>). (a) 0 h. (b) 23 h. (c) 29 h. (d) 35 h. (e) 44 h. (f) 50 h.

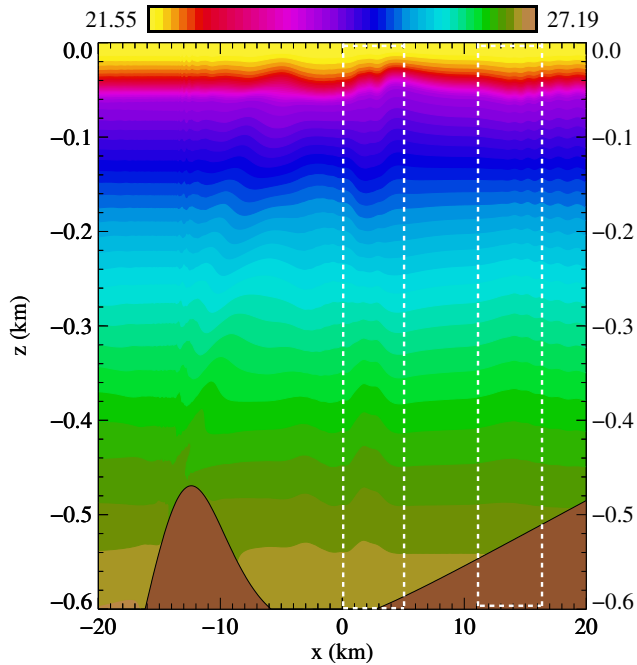


**Figure 8.** Density field for same case and time shown in Fig. 7c showing mode-two waves (in white dashed boxes) and an internal wave beam (above the bump) generated when the solitary wave passes over the bump.

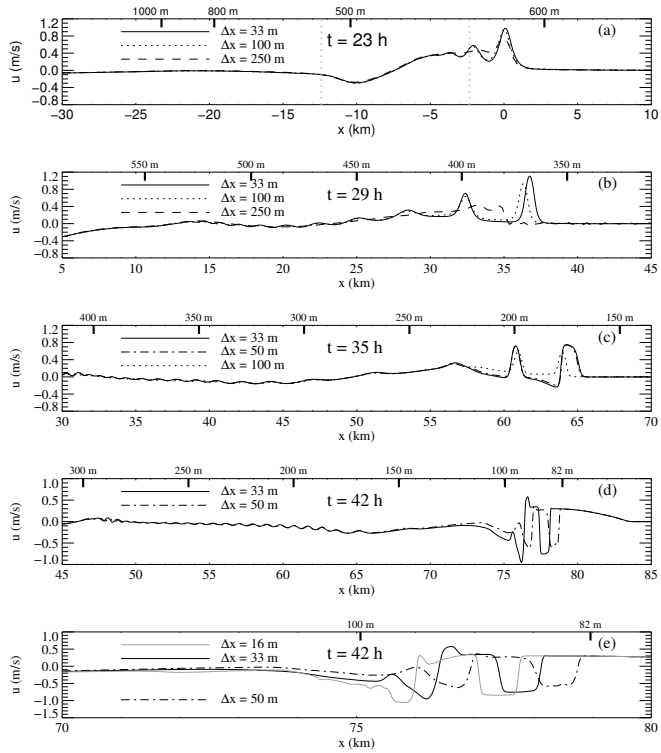




**Figure 9.** Resolution ~~testtest~~ results. Shown are surface currents at four different depths for Case 3 ~~which uses~~ bathymetry  $h_{15}$  and ~~an~~ initial wave amplitude of 45 m. Panels compare results from simulations with different horizontal resolutions using 200 grid points in the vertical:  $\Delta x = 33$  (solid), 50 (dash-dot, **c**, **d** only), 100 and 250 (dashed, **a**, **b** only). **(a)**  $t = 23$ . Leading wave at 610 m depth – see Fig. 7b. **(b)**  $t = 29$  h. Leading wave at 370 m depth – see Fig. 7c. **(c)**  $t = 35$  h. Leading wave at 180 m depth – see Fig. 7d. **(d)** Results at  $t = 42$  h. First depression in water shallower than 82 m. Second depression at 90 m depth. ~~(d) Also includes results from simulation with  $\Delta x = 33$  (e) Zoom in on leading waves at  $t = 42$  and  $J = 400$  points h. Vertical dashed lines in panel (dotted a). This curve is indistinguishable from indicate the solid curve location of the crest of bump and the depth maximum between the bump and the shelf. Depths are indicated by black marks along upper axis.~~

~~Bathymetry used for adiabatic shoaling tests with initial depths of 3000 (solid), 1500 (dashed) and 1000 (dots). Shallow water depth is 80.~~

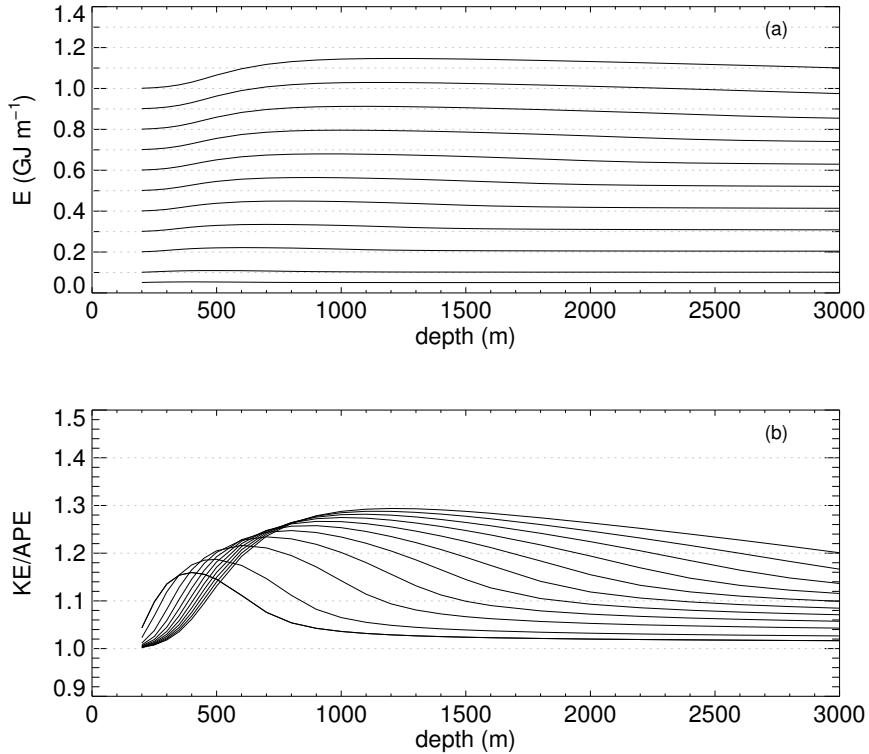


**Figure 10.** (a) Total ISW energy (APE plus KE) for ISWs with fixed APE as a function of water depth. Curves are for APE equal to  $25 \text{ MJ m}^{-1}$  and  $50 \text{ MJ m}^{-1}$  to  $500 \text{ MJ m}^{-1}$  in increments of  $50 \text{ MJ m}^{-1}$ . (b) Ratio of KE to APE for same waves. On right side the ratio increases with APE.

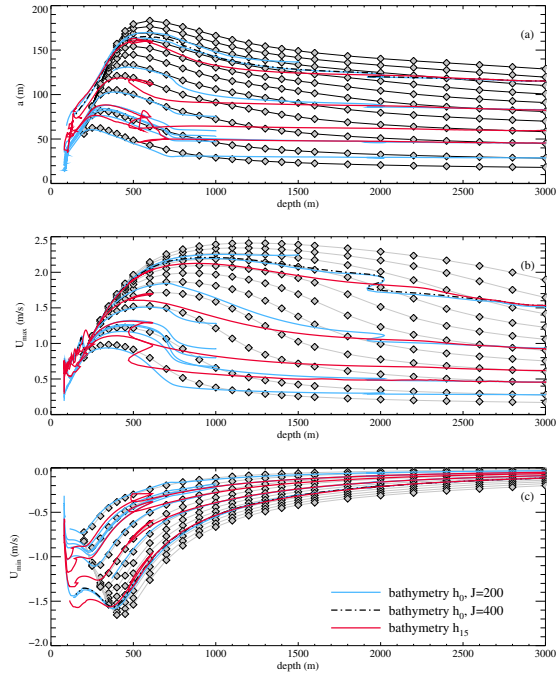


**Figure 11.** Wave properties as a function of water depth. **(a)** Wave amplitudes (absolute value), **(b)** maximum surface currents, **(c)** minimum bottom currents. **Black-Grey** curves with **grey** diamonds are for ISW solutions of the DJL equation for waves with total energy  $E$  equal to  $50 \text{ MJ m}^{-1}$  and  $100$  to  $1000 \text{ MJ m}^{-1}$  in increments of  $100 \text{ MJ m}^{-1}$ . Diamonds indicate computed values. Coloured curves are maximum absolute amplitude and surface current and minimum bottom currents of shoaling waves as function of water depth. Blue – cases using bathymetry  $h_0$ . Red – cases using bathymetry  $h_{15}$ . **Green-dotted-Black dash-dot** – higher resolution case **started at depth of 3000** using bathymetry  $h_0$ . This curve overlies the lower resolution result (blue curve, initial amplitude 115 m). Both are overlain by the results using bathymetry  $h_{15}$  for depths greater than about 2600 m.

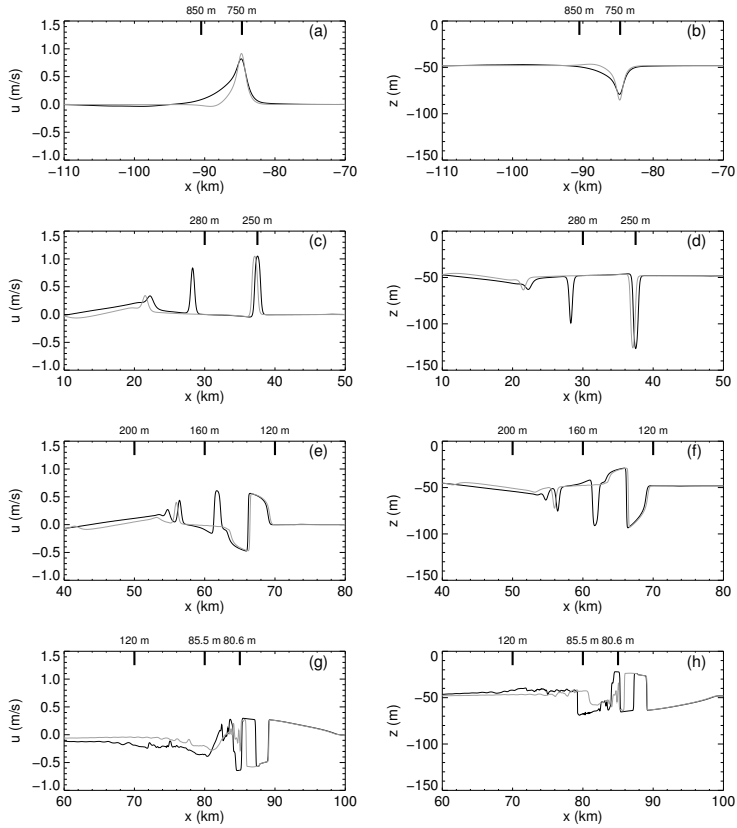


**Figure 12.** Horizontal velocity-Surface current (left) and  $\sigma_t = 0.0232 \text{ kg m}^{-3}$  isopycnal (right) at the surface at different times for waves with initial APE of 100 and 60  $\text{MJ m}^{-1}$  started at depths of 3000 (solid) and 1000 m (dashed) respectively using bathymetry  $h_0$ . Times are different for the two waves, chosen so that the leading waves are at approximately the same location. Leading waves at depth of: (a) 750; (b) 560; (c) 250; (d) 135–120; (e) 90–80 depth; and (f) 80 Sample local depths are indicated along the upper axis.

The  $\sigma_t = 0.0232$  isopycnal. Same cases and times as in Fig. ??.

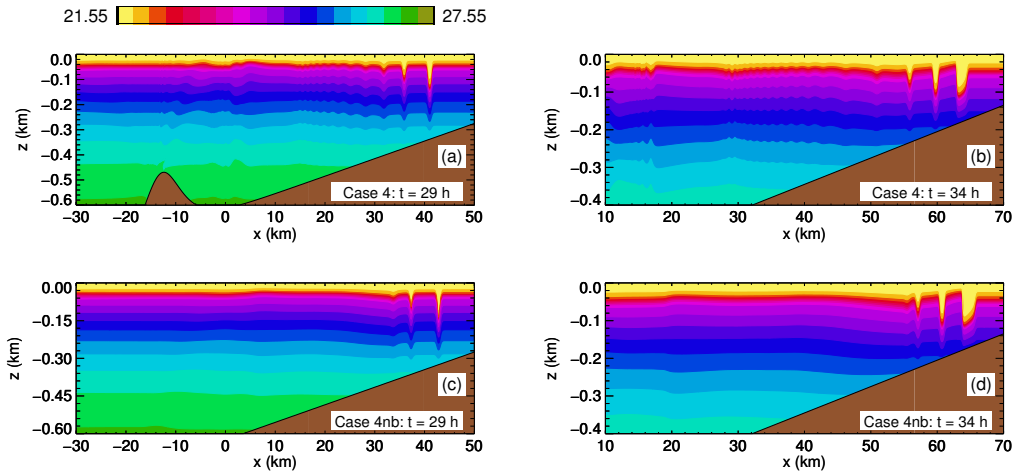


**Figure 13.** Effects of the bump for bathymetry  $h_{15}$ . Initial amplitude 59 m (Cases 4 and 4nb). **(a, b)** Bathymetry  $h_{15}$ . **(c, d)** Bathymetry  $h_{15}$  with bump removed. **Times: (a, c)  $t = 29$ . (b)  $t = 34$ . (d)  $t = 33$ h and 40min.**

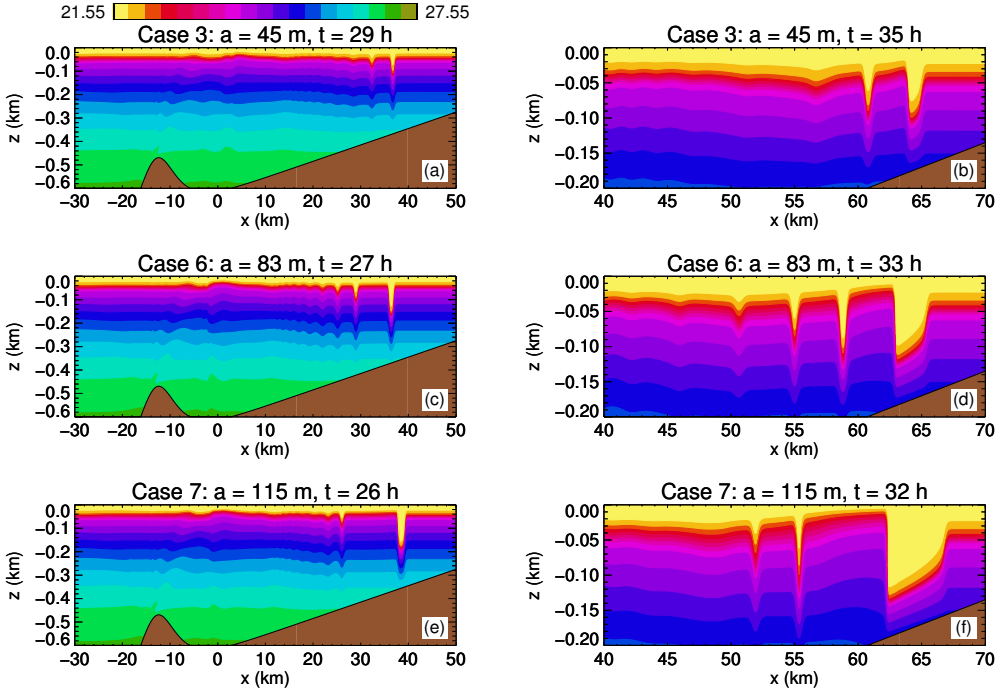


**Figure 14.** Density fields for shoaling waves with different initial wave amplitudes using bathymetry  $h_{15}$  and stratification  $\bar{\rho}_b$ . **(a, b)** Case 3. Initial amplitude  $a = 45$ : results at  $t = 29$  and  $t = 35$ . **(c, d)** Case 6. Initial  $a = 83$ . Results at  $t = 28$  and  $t = 34$ . **(e, f)** Case 7. Initial amplitude  $a = 115$ . Results at  $t = 27$  and  $33$ .

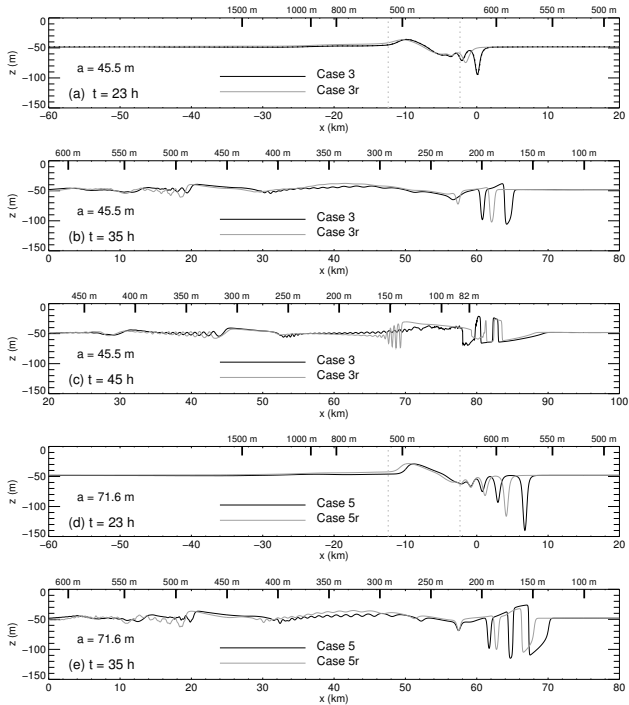


**Figure 15.** Effects of rotation are illustrated by comparing the  $\sigma_t = 0.0232 \text{ kg m}^{-3}$  isopycnals for two different initial waves. Base stratification with bathymetry  $h_{15}$ . **(a, c)** **(a, b, c)** Cases 3 and 3r: initial wave amplitude is 45.4 m ( $\text{APE} = 100 \text{ MJ m}^{-1}$ ). **(b, c)** **(d, e)** Cases 5 and 5r: initial wave amplitude is 71.6 m ( $\text{APE} = 200 \text{ MJ m}^{-1}$ ). Solid black curves are results without rotational effects. Dashed curves are results with  $f = 5.35 \times 10^{-5} \text{ s}^{-1}$ . Results are shown at times **(a, b)**  $t = 23$  h and **(c, d)**  $t = 35$  h. Vertical dashed lines indicate the location of the crest of bump and **(c, d)**  $t = 35$  h. The resolution for these results was  $\Delta x = 33$  m and  $J = 200$ . Also plotted are results obtained using  $\Delta x = 33$  m and  $J = 400$  for  $f = 0$  indicated by black marks along upper axis. These curves are indistinguishable from the lower resolution results.



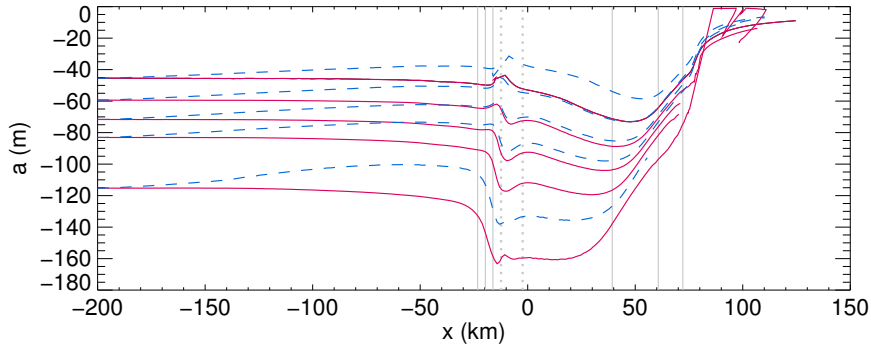


**Figure 16.** Effects of rotation on the amplitude of the leading wave as a function of  $x$ . Bathymetry  $h_{15}$ . Solid red curves: cases without rotation. Dashed blue curves: cases with rotation. Cases 3–7 and 3r–7r. The solid vertical grey lines indicate locations where water depth is 1000, 800, 600 (first occurrence), 350, 200 and 120 m. The vertical dashed lines indicate the locations of the top of the bump at  $x = -12.4$  km (480 m depth) and maximum depth (618 m) up shelf of it.

Comparisons of wave fields using observed stratifications for  $APE = 50$  and bathymetry  $h_{15}$ .  $f = 0$ .  
**(a, c, e)** Case 8: density  $\bar{\rho}_1$ . **(b, d, f)** Case 11: density  $\bar{\rho}_2$ . **(a)**  $t = 36$ . **(b)**  $t = 38$ 10. **(c, d)**  $t = 47$ . **(e,**  
**f)**  $t = 55$ .

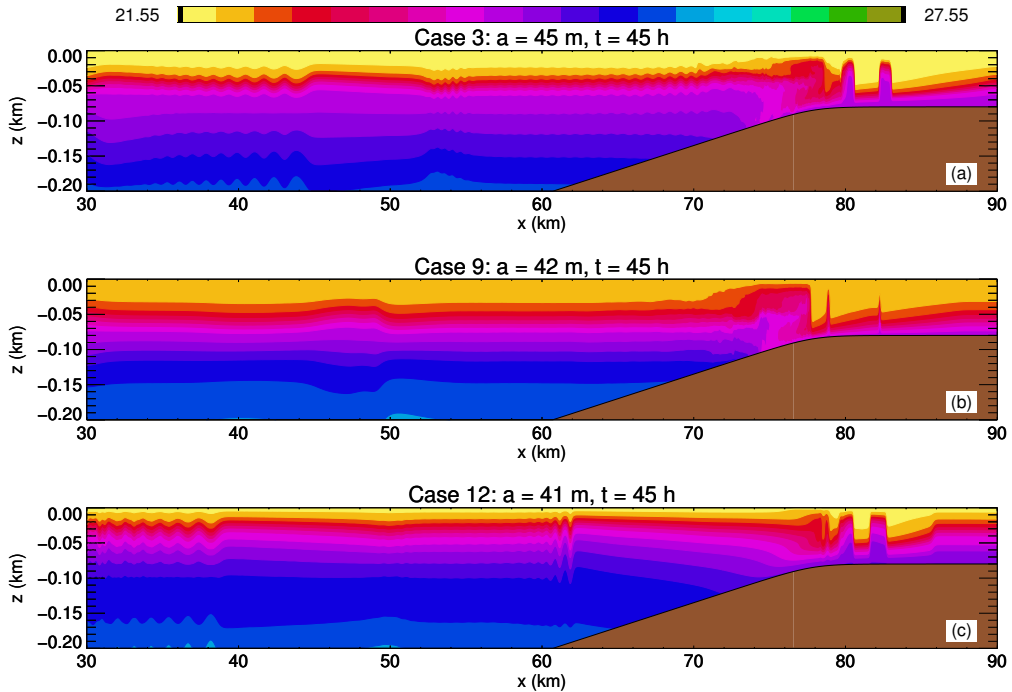


**Figure 17.** Comparisons of wave fields using observed stratifications for  $APE = 100 \text{ MJ m}^{-1}$  and bathymetry  $h_{15}$ .  $f = 0$ . **(a)** Case 8: density  $\bar{\rho}_1$ . **(b)** Case 9: density  $\bar{\rho}_1$ . **(c)** Case 12: density  $\bar{\rho}_2$ .

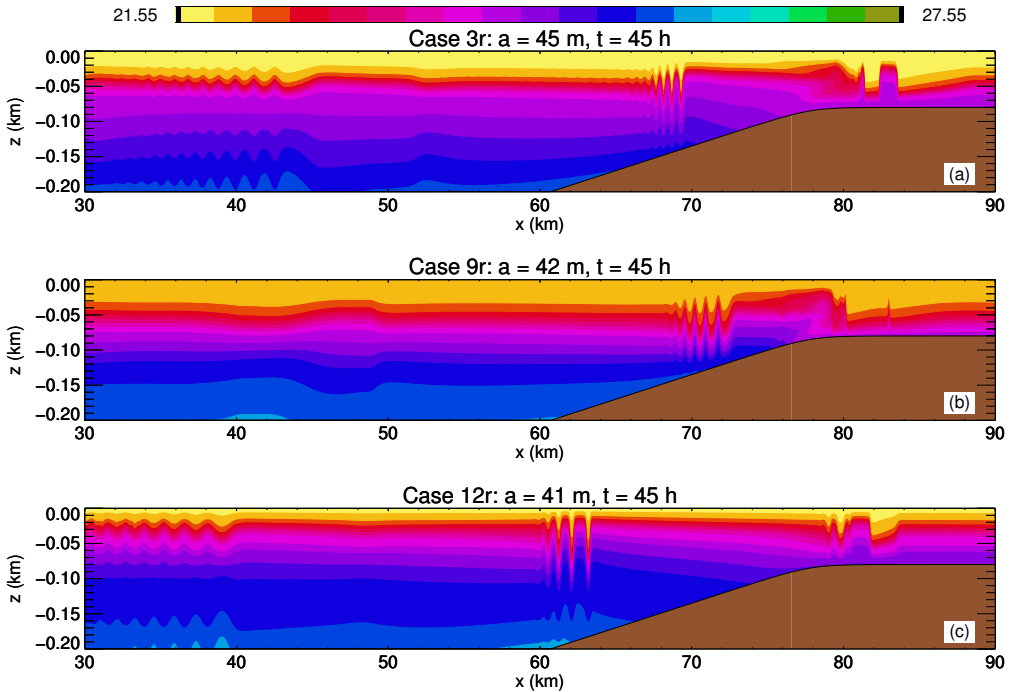


**Figure 18.** Same as previous figure but with  $f = 5.33 \times 10^{-5} \text{ s}^{-1}$  (Cases 8r and 11r) and (c, d) are at  $t = 43$ .

The vertical diffusivity profile function  $f(z)$ .

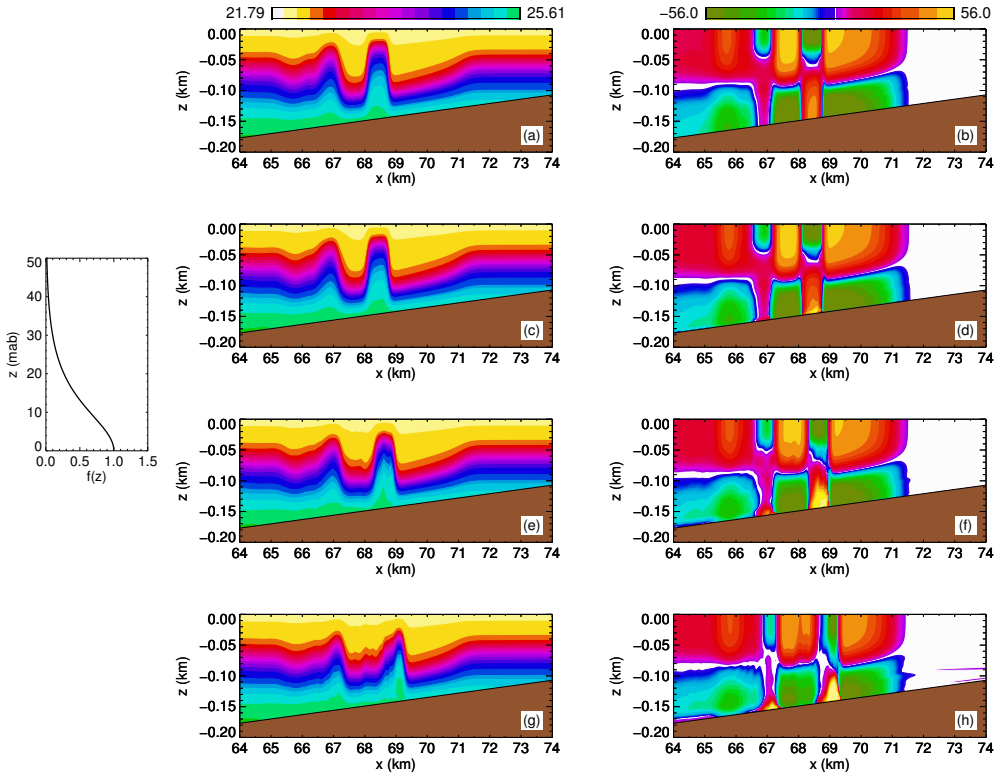


**Figure 19.** Effects of viscosity on shoaling waves. Stratification  $\bar{\rho}_1$ , initial wave amplitude  $41.7 \text{ m}$  ( $\text{APE} = 100 \text{ MJ m}^{-1}$ ). Left panels show column shows the density field ( $\sigma_\rho$ ), right panels show column shows the corresponding horizontal velocity (in  $\text{cm s}^{-1}$ ). For the velocity fields the red-orange-yellow colours indicate positive (on shelf) currents while green-blue indicate negative currents. Left inset shows the eddy viscosity/diffusivity profile function  $f(z - z_b)$ . (a, b) Inviscid. (c, d)  $K = 1.0 \times 10^{-5} \text{ m}^2 \text{ s}^{-1}$ . (e, f)  $K = 1.0 \times 10^{-4} \text{ m}^2 \text{ s}^{-1}$ . (g, h)  $K = 1.0 \times 10^{-3} \text{ m}^2 \text{ s}^{-1}$ .